AD NUMBER

AD902342

NEW LIMITATION CHANGE

TO

Approved for public release, distribution unlimited

FROM

Distribution authorized to U.S. Gov't. agencies only; Test and Evaluation; MAR 1972. Other requests shall be referred to Air Force Armament Lab., Eglin AFB, FL.

AUTHORITY

USADTC ltr, 6 Feb 1979

AD902342

AFATL-TR-72-44

STUDIES OF THE DYNAMIC FRACTURE CHARACTERISTICS OF COMPOSITES

DEPARTMENT OF ENGINEERING
SCIENCE AND MECHANICS
UNIVERSITY OF FLORIDA

TECHNICAL REPORT AFATL-TR-72-44

MARCH 1972

AIR FORCE ARMAMENT LABORATORY
AIR FORCE SYSTEMS COMMAND • UNITED STATES AIR FORCE
EGLIN AIR FORCE BASE, FLORIDA

Studies Of The Dynamic Fracture Characteristics Of Composites

R.L. Sierakowski
G.E. Nevill, Jr.
C.A. Ross
E.R. Jones

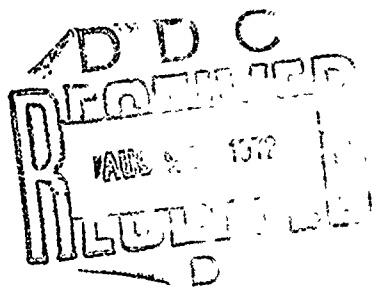

FOREWORD

This final report documents research accomplished during the period January 1970 to January 1971 by the Department of Engineering Science and Mechanics, University of Florida, Gainesville, Florida, under Contract F08635-71-C-0076 with the Air Force Armament Laboratory, Eglin Air Force Base, Florida. Mr. Leonard L. Wilson (DLRD) was program monitor for the Armament Laboratory.

This technical report has been reviewed and is approved.

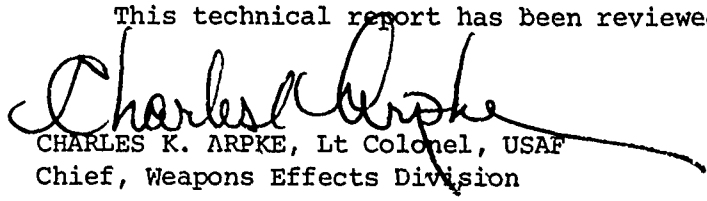

CHARLES K. ARPKE, Lt Colonel, USAF
Chief, Weapons Effects Division

ABSTRACT

The wave propagation behavior of composite bar specimens of variable fiber spacing and orientation is investigated. In addition, controlled geometry composite plates have been fabricated and impact tested to determine their failure/fracture characteristics. Wave propagation studies have been conducted on long rods with single filament lamina as well as continuous filament composite rods with variable filament orientation. A square wave input has been introduced into the rods, and wave speed, attenuation, and dispersion have been investigated. Analytical criteria have been considered to model a single lamina composite bar in order to isolate the influence of a single interface on wave speed, attenuation and dispersion. These results have been examined for correlation with multiple filament rods. Various geometry plate specimens have been fabricated and impact tested to determine their energy-absorbing characteristics and failure/fracture modes. Further, penetrator specimens of a model composite geometry type have been impact tested against variable density targets to investigate the possibility of producing controlled fracture characteristics.

(The reverse of this page is blank.)

TABLE OF CONTENTS

LIST OF FIGURES

LIST OF FIGURES (CONTINUED)

LIST OF FIGURES (CONCLUDED)

LIST OF TABLES

(The reverse of this page is blank.)

SECTION I

INTRODUCTION

The studies reported herein are directed toward understanding the wave propagation behavior of composite-type materials for application to terminal ballistics design.

The laboratory development of super high strength fiber and associated fabrication techniques has resulted in new material design applications. Since material systems are exposed to a wide variety of loading problems, it is important to develop an understanding of static and dynamic material response characteristics. One technologically important area of study is related to the dynamic impact process at the high strain rates associated with stress waves. It is therefore important to identify and classify those constituent and geometrical material characteristics which are significant. Further, the inherent heterogeneity of composite materials gives rise to new mechanisms of failure and fracture.

Past efforts described in References 1 and 2 have been directed toward establishing basic information on the material properties and mechanisms which appear as important design parameters. The present program is a continuation of the effort to systematically evaluate important dynamic material properties. In addition, information generated from previous and current studies have been examined in relation to the potential controlled fracture behavior of the terminal ballistic problem. While the potential combinations of various types of composite materials is unlimited, principal attention has been focused on a single model system. The system selected for continued study is the steel-epoxy composite. It has been demonstrated by past efforts that carefully controlled specimens of varying geometrical shapes, orientations, and fiber sizes can be readily prepared in the laboratory. In addition to this system, other types of composites have been fabricated and or obtained from outside sources for comparative evaluation with the model system.

One aspect of the present experimental program has involved wave propagation studies including acoustic velocity measurements, amplitude attenuation, and wave dispersion. These studies have been conducted on carefully fabricated long bar specimens with single and multiple filament constituents. The pulse shape introduced into the specimen is a rectangle pulse reprsentation of the type imparted during plate impact. Test configurations have been selected in order to investigate such geometric effects as filament size, spacing, and orientation. In addition, the isolated influence of a single lamina with variable geometric properties has been studied for prediction of multiple filament response characteristics. The above mentioned studies are of basic importance to understanding compressive fracture mechanisms since the relationship of pulse attenuation to such fracture may be

significant, as discussed in Reference 3. In order to establish meaningful and simplistic type test procedures, a series of measurements on laboratory-prepared axial composite beam specimens of the same geometrical variation as the long bar specimens has been studied. These investigations have been directed toward measuring pulse attenuation and pulse velocity as a function of frequency in order to predict the pulse propagation in a long bar specimen. Such test procedures would be advantageous in screening the potential fracture characteristics of candidate composite materials.

The second phase of the current test program has been directed toward investigating the use of composites in terminal ballistics applications. One aspect of this program has been concerned with the failure/fracture of composite plate-type specimens impacted by a steel penetrator. Geometrical variation of plate geometry has been studied on several types of composite plate configurations for fracture characterization. The second part of this study has been concerned with the practicality of establishing controlled fracture of axial and transverse fialment steel-epoxy penetrators. This model system has been investigated against plate materials of variable ductility, mass, and strength with specimen failure and fracture observed.

SECTION II

WAVE PROPAGATION STUDIES

2.1 Introduction

One of the principal problems encountered in dynamic loading processes is that of determining how short duration pulses are propagated through the material. That is, in impact processes energy may be transmitted large distances from the point of impact by stress waves which can produce considerable damage at remote distances from the impact point. Thus, in order to predict and control the type and extent of the fracture phenomenon, at the high strain rates associated with stress waves, knowledge of the dynamic properties and stress wave propagation in the material is of importance. Included in such studies are important composite parameters such as reinforcement spacing, orientation, material properties, and interrelationships among various wave characteristics.

Analytical and experimental studies of the dynamic response and stress pulse propagation in homogeneous and isotropic materials have been investigated, and discussed in References 4 and 5. An extension of the above theories to composite materials is complicated due to the mathematical difficulty in developing appropriate solution techniques. For this reason, it is desirable to generate carefully controlled experimental data on material properties over a wide range of environments in order to select and establish the important response parameters.

At the present time, experimental studies in the area of dynamic properties of composite materials have been directed toward investigating the overall response of a class of technically important composites of the filamentary type. The response of such composites has been examined from the point of view that the properties can be described by some experimentally or analytically determined average. Once the constituent properties are determined, it is then necessary to relate these characteristics to those of the overall composite material. The most often used method of doing this is through the rule of mixtures [6]. This method has been found to be especially useful in determining such material properties as density and modulus of elasticity [6,7].

This approach has been less successful in predicting the strength characteristics of composite materials. However, it has been shown that wave propagation speeds in some composites follow such a rule as demonstrated in References 2 and 8. Other important dynamic properties such as wave attenuation, dispersion, and material damping have been found to be related to a combination of parameters, for example, material geometry [9], constituent material properties [10], and wave propagation velocity [8,10].

Some pulse propagation and attenuation studies for impact-generated pulses in axially reinforced bars have been reported in References 2,11-13. Additional dynamic wave characteristics, such as dispersion and attenuation along with their dependence on transmission frequency, are discussed in References 10 and 12.

The principal objectives of this study are to establish experimental techniques supplemented by appropriate analytical models for examining the propagation of impact-generated pulses through composite-type materials. Included in the studies are the effects of such composite parameters as filament size, spacing and distribution on wave speed, energy dissipation, and wave dispersion.

In order to obtain information for control of the failure/fracture process, the impact of long bar specimens with longitudinal and transverse distributed filaments has been examined. An additional investigation of the influence of a single layered interface on the pulse propagation, attenuation, and dispersion has been studied in order to predict both experimentally and analytically the type of results expected from continuously distributed interface systems. For these tests the model steel-epoxy system has been used in order to relate to previously established data.

2.2 Wave Propagation in Rods with Single Transverse Layers

To evaluate the overall results of pulse propagation tests on multiple transverse layered bars, studies of the wave propagation through a single layer in a long bar specimen have been investigated.

2.2.1 Specimen Fabrication

Several fabrication schemes were devised and tried before an effective process was devised. The fabrication process found to be most consistent with reproducibility is reported on. Several other schemes tried but with less success are reported on for completeness in Reference 14.

The basic assembly used for casting the long bar specimens is the mold shown in Figure 1. This mold consisted of an 81.28×10^{-2} meters long by 1.27×10^{-2} meters square channel with a clamp located at the center to hold the grid gate.

The grid gate, as shown in Figure 1, was fabricated using type 304 stainless steel wire with a nominal diameter of 0.02×10^{-2} meters and was wound on a mandrel using a lathe. The thread-cutting cross feed of the lathe was used to control the spacing of the wires on the mandrel. After winding, the wires were cleaned with acetone and bonded to the gate with epoxy cement. Following curing of the cement, the mandrel and excess wire were removed, and the entire assembly was cleaned in a trichloroethylene vapor bath.

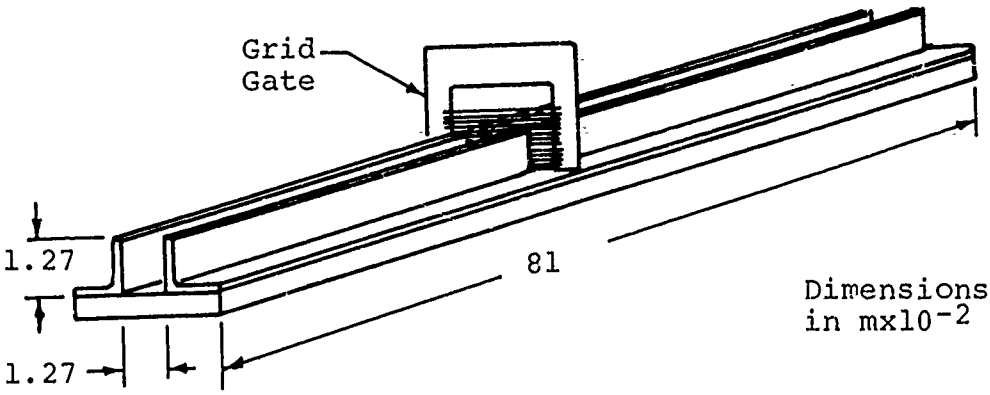

Figure 1. Mold Assembly

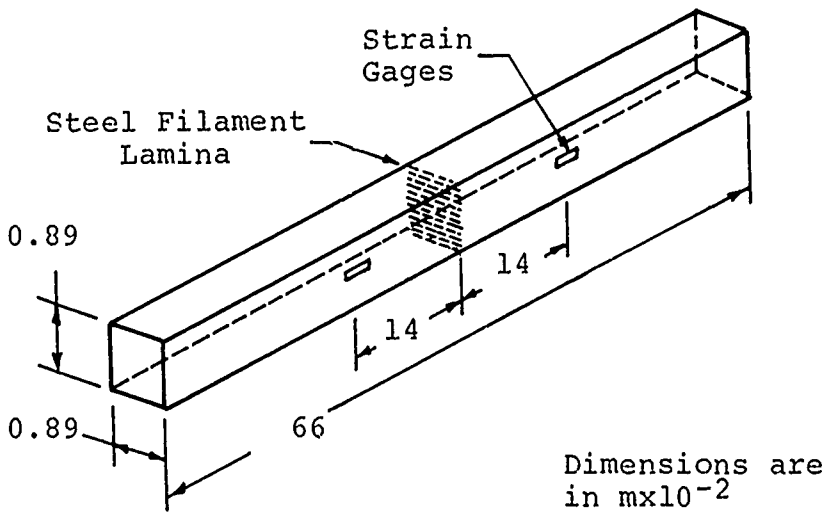

Figure 2. Schematic of Instrumented Specimen

From previous work, it was determined that the interface bond between the filaments and matrix was unsatisfactory due to the trichloroethylene vapor cleaning procedure. Therefore, after the gates had been fabricated, a specific procedure, as described below, was used to clean them. This consisted of (a) degreasing with acetone, (b) rubbing each side several times with a grit (600) polishing paper soaked in acidic metal cleaner followed by wiping with gauze, (c) cleaning with gauze soaked with metal cleaner, and (d) dipping in ammonia solution followed by thorough wiping with clean gauze. The procedure described was found to produce enhanced bond strengths for the fabricated specimens.

The specimen blanks were prepared from the mold assembly as follows. First, the mold was cleaned and spray coated with teflon release agent for easy specimen removal. The cleaned gate was inserted in the mold assembly, and the entire system was furnace preheated to 65.5°C. Shell Epon 828 resin was preheated to 65.5°C mixed with twelve parts per hundred of type 400-A hardener, degassed for 20 minutes in vacuum (25mm Hg), and poured into the mold assembly. The entire system was cured at 65.5°C for three hours. After curing, the excess grid work was first removed and the specimen blanks machined to the final nominal dimensions of 0.89×10^{-2} meters square by 66.05×10^{-2} meters long. Selection of a square specimen geometry was based upon difficulty in fabricating an acceptable circular bar-type specimen. According to Reference 5, however, the square cross-section geometry is equivalent to a 0.97×10^{-2} meters round section in acoustic velocity. Using the above procedure, the following specimens were fabricated, (a) pure epoxy bar with no lamina, (b) single lamina specimens with wire densities of 12.6, 18.9, 31.5, 44.1, 49.3 wire/m$\times 10^{-2}$, and (c) a specimen with three laminae equally spaced at 16.5×10^{-2}m having 18.9 wires/m$\times 10^{-2}$.

2.2.2 Experimental Procedure

The finished specimens were instrumented using BLH FAE-065-1236 etched foil strain gages, as shown in Figure 2, with the active gage placed in a bridge circuit, as shown in Figure 3. It was found necessary to limit the current in the strain gage to less than five milliamperes due to low thermal conductivity of the epoxy. Initial tests were performed, using an air gun assembly described in Reference 1, to propel a round projectile against a round specimen; however, the simpler system shown schematically in Figure 4 permitted the use of a square projectile and a square cross-section rod. Small amplitude square pulses were generated in the specimen by impacting it with a 0.0763-meter-long epoxy projectile of the same cross-sectional dimensions as the specimen. Pulse shape and wave propagation speed were monitored using the strain gage output connected to an oscilloscope. Most specimens were instrumented with two equally spaced strain gages located at both sides of the lamina.

In these cases the first pulse was used to trigger the oscilloscope by the internal trigger mode and with proper adjustment the major portion of the pulse was recorded. The second strain gage was then recorded on the other

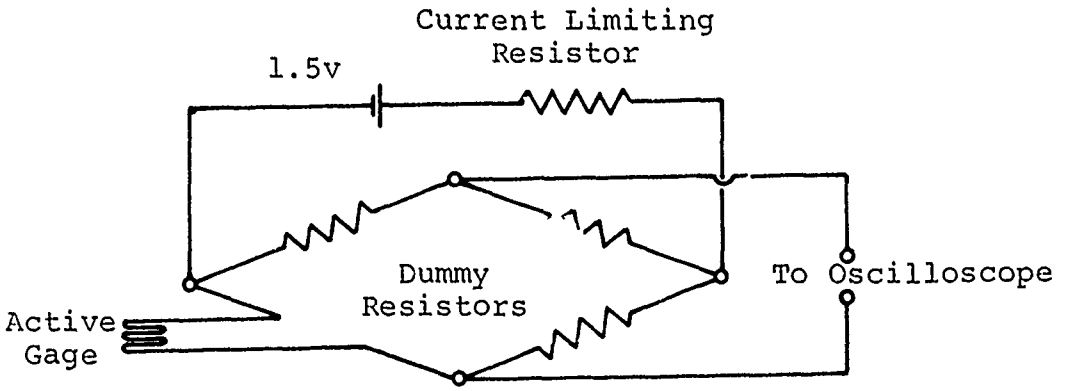

Figure 3. Wheatstone Bridge Strain Gage Circuit

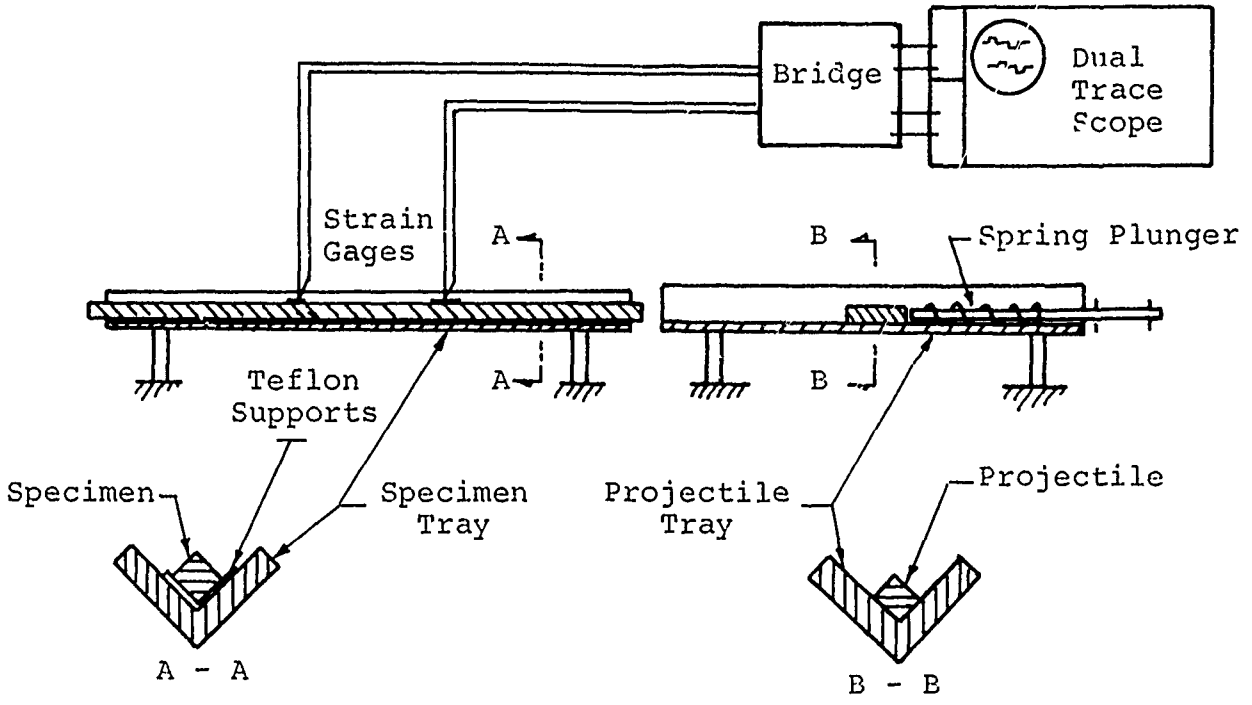

Figure 4. Low-Speed Impact Test Apparatus for Transversely Reinforced Bars

beam and, in turn, gave pulse shape changes both before and after the lamina. Typical pulse shape changes showing the initial compressive pulse and the first reflected tensile pulse are shown in Figure 5. A multiple reflection record of the pulse attenuation is also included in Figure 6. The above oscillograph traces were recorded using a Polaroid camera attachment.

2.2.3 Wave Speed, Attenuation, and Dispersion

The pulse propagation speed was calculated using typical data, as shown in Figure 6. The initial compressive peak was selected as a reference, and from the measured rod length and time between successive peaks, the pulse propagation speed was calculated for the second, fifth, and tenth traverses of the rod. A summary of the results obtained are given in Table I.

TABLE I. AVERAGE PULSE PROPAGATION SPEEDS IN TEST SPECIMENS AFTER 2, 5, AND 10 COMPLETE CYCLES

Filament Density (1/meter $x10^{-2}$)	c_2 m/sec	c_5 m/sec	c_{10} m/sec
0	1,834	1,852	1,877
12.6	1,826	1,849	1,875
18.9	1,824	1,842	1,869
31.5	1,821	1,816	1,836
44.1	1,821	1,821	1,836
49.3	1,806	1,814	1,831
18.9*	1,808	1,806	1,816

*Indiates specimen with 3 - $18.9x10^2$ filaments per meter laminae.

The peak-to-peak amplitude decrease, referred to as the attenuation, was defined as the natural log of the pulse amplitude ratio divided by the rod length traversed between the two pulses. For the tests reported here, using the rod length and initial pulse amplitude, the attenuation was determined from

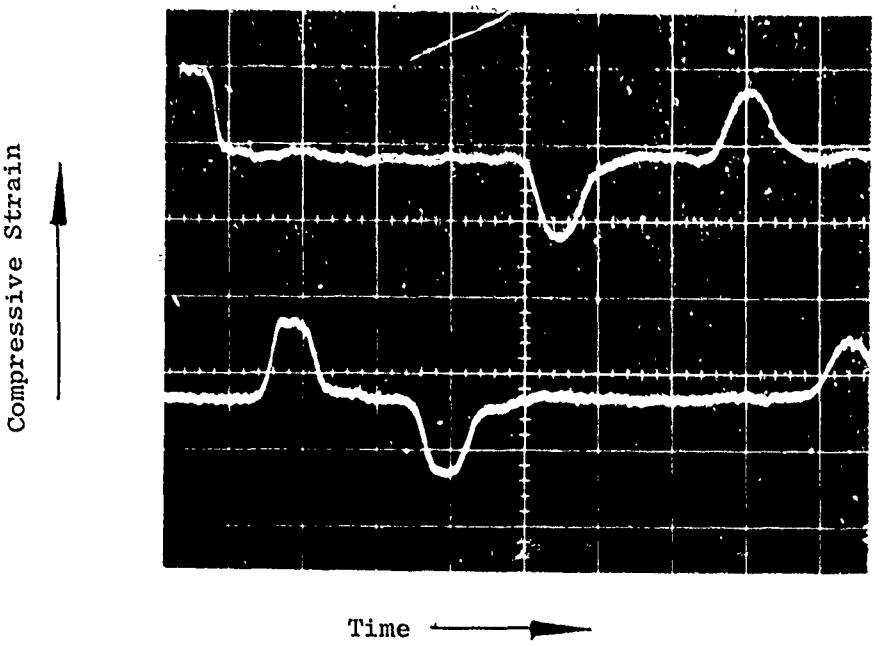

Figure 5. Initial Compressive and Tensile Pulses Before and After Lamina

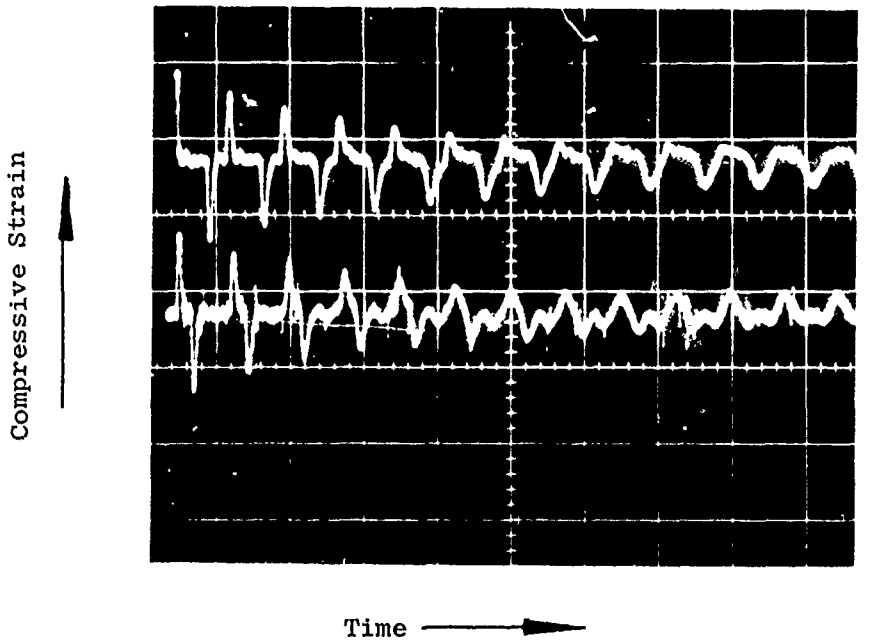

Figure 6. Multiple Reflection Pulse Attenuation

$$D = \frac{1}{2n\ell} \ln \left[A_o / A_n \right] .$$

Amplitude attenuation calculated for n = 2, 5, and 10 cps are shown in Table II and graphically in Figure 6. In order to further identify and isolate the influence of a single lamina on pulse attenuation, a factor δ_n, called the lamina attenuation, has been introduced. This factor is defined as

$$\delta_n = (D_n - D_{ne})L$$

where, δ_n is the attenuation of a single lamina after n cycles, D_n is the attenuation after n cycles in a specimen with a lamina, D_{ne} is the attenuation after n cycles in a pure epoxy bar, and L is the average distance the pulse travels between lamina passages. A summary of experimentally determined lamina attenuation values is given in Table III.

TABLE II. AVERAGE PEAK-TO-PEAK AMPLITUDE ATTENUATIONS IN TEST SPECIMENS AFTER 2, 5, AND 10 COMPLETE CYCLES

Filament Density (1/meter x10^{-2})	D_2x10 (1/meter)	D_5x10 (1/meter)	D_{10}x10 (1/meter)
0	0.71	0.64	0.59
12.6	0.80	0.69	0.64
18.9	0.87	0.73	0.66
31.5	0.92	0.76	0.68
44.1	0.94	0.78	0.69
49.3	0.95	0.79	0.72
18.9*	1.00	0.87	0.81

*Indicates specimen with 3 - 18.9x10^2 filaments per meter laminae.

TABLE III. AVERAGE LAMINA ATTENUATION NUMBERS AFTER 2, 5, AND 10 COMPLETE CYCLES

Filament Density (1/meter $x10^{-2}$)	$\delta_2 x10^3$	$\delta_5 x10^3$	$\delta_{10} x10^3$
12.6	5.72	3.38	3.38
18.9	14.0	[illegible]	4.94
31.5	13.9	7.80	6.24
44.1	15.1	9.38	8.06
49.3	15.6	10.1	8.58
18.9*	6.20	5.03	4.94

*Indicates specimens with 3 - $18.9x10^2$ filaments per meter laminae.

The dispersion and shape change of pulses have also been considered. In particular, typical pulse shape changes obtained during the first, seventh, and eleventh cycles with different scales are shown in Figure 7. A schematic representation of the pulse shape changes is shown in Figure 8 where the waveforms have been superimposed. It is observed that the pulse shape is relatively little changed between the seventh and eleventh cycles. Considering that pulse shape is little changed after a certain number of cycles, it appears that amplitude attenuation should reach an asymptotic value after a large number of cycles. The previously defined amplitude attenuation has been recast in the form

$$D(n) = \beta e^{-\gamma n} + \alpha$$

where β, γ, and α are experimentally determined constants. Since the values of D_n have been determined for n = 2,5, and 10, the values of β, γ, and α are determined. Using the value of α in place of D_n in the equation determining the lamina attenuation, this factor has been re-evaluated. These data are presented in Table IV and are plotted graphically in Figure 9. Other data presented in Table IV and Figure 9 have been determined by analytical techniques which are described briefly in this section and in detail in Appendix I. The physical phenomenon involved in the pulse attenuation through a transverse fiber interface is a complex occurrence involving

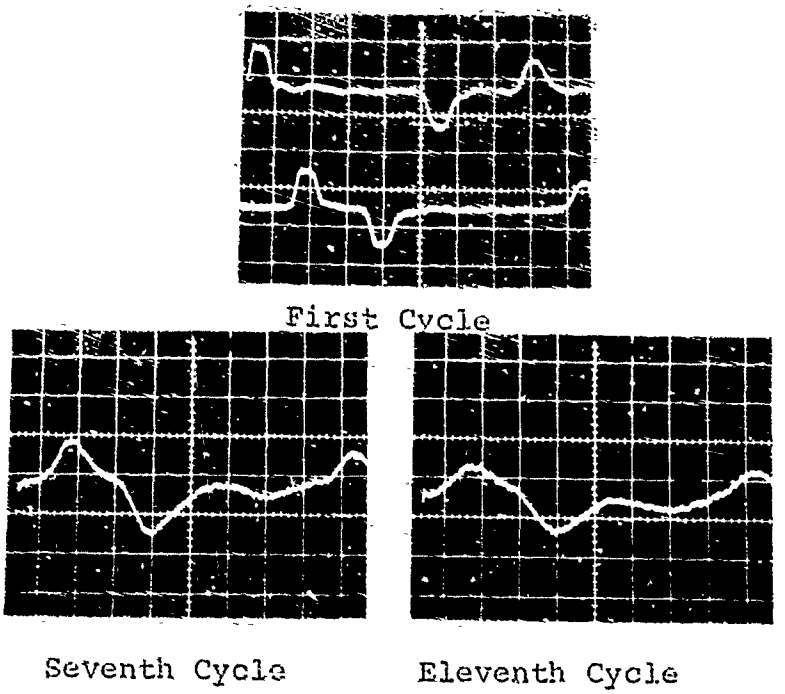

Figure 7. Waveform Photographs for Single Composite Lamina Specimens

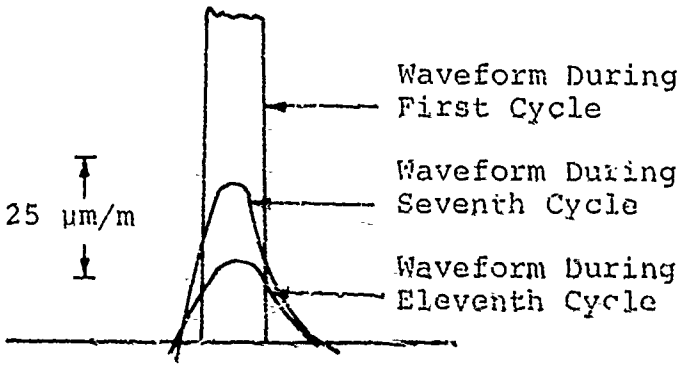

Figure 8. Schematic of Waveforms

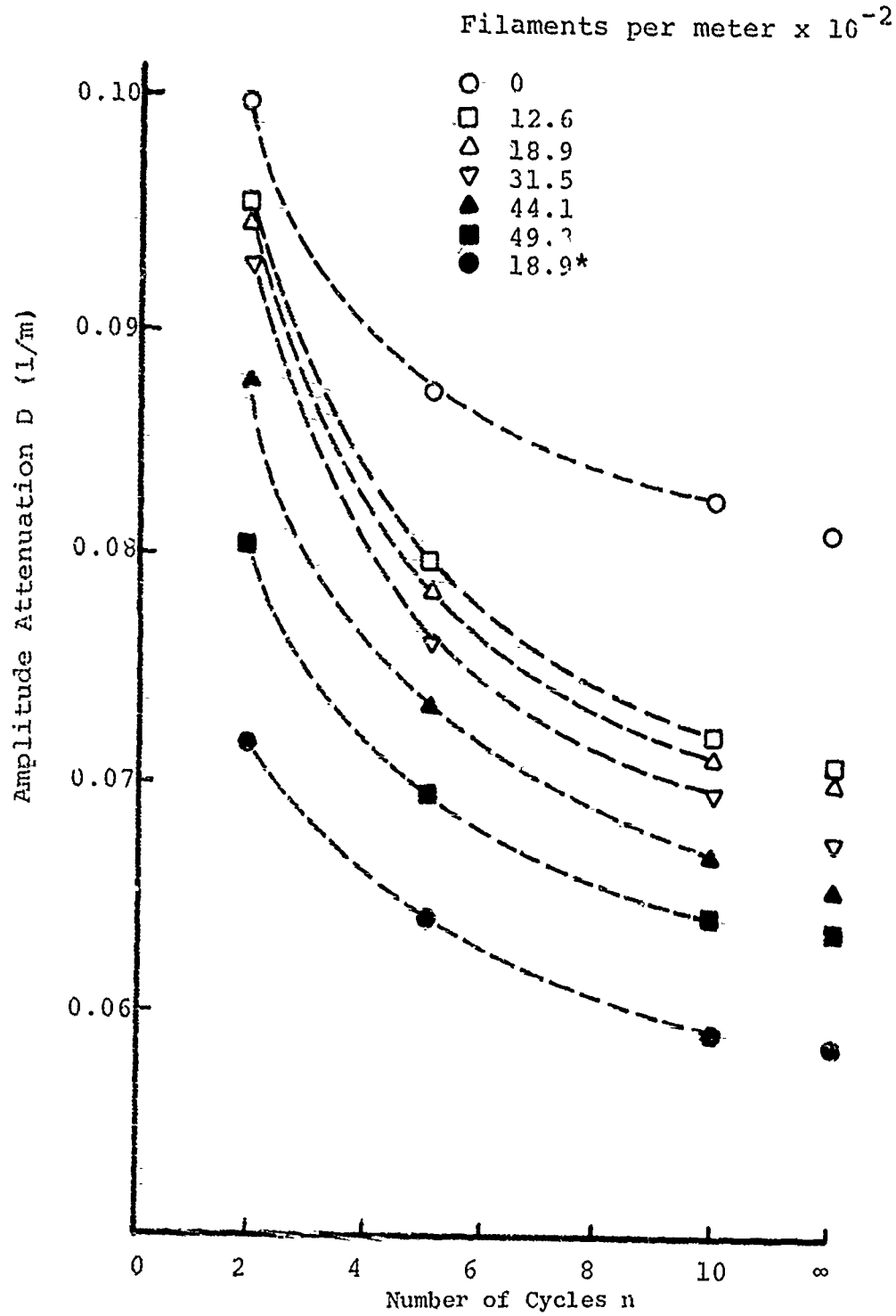

Figure 9. Attenuation Versus Travel Distance

pulse reflection, transmission, and scattering. Therefore, several analytical approaches have been formulated in an attempt to describe the observed phenomena.

TABLE IV. ASYMPTOTIC ATTENUATION, LAMINA ATTENUATION VALUES, AND PREDICTED LAMINA ATTENUATION NUMBERS FOR TEST SPECIMENS

Filament Density (1/meter $x10^{-2}$)	$\alpha x10$ (1/meter)	$\delta x10^{3}$	$\delta_1 x10^{3}$
0	0.58	0	
12.6	0.63	3.12	2.10
18.9	0.65	4.42	5.62
31.5	0.67	5.72	8.13
44.1	0.69	7.28	0.00
49.3	0.70	8.06	9.64
18.9*	0.80	4.86	

*Indicates specimens with 3 - $18.9x10^{2}$ filaments per meter laminae.

One such approach models the transverse interface as an equivalent new material, the properties of which are determined by the rule of mixtures. Using one-dimensional wave theory and considering that no internal reflection/transmission takes place in the lamina, an analytic attenuation factor denoted by the symbol δ_1 has been obtained. It should be noted that the transverse acoustic velocity as determined for a homogeneous-anisotropic material has been used in the calculations. This model predicts an optimum value of attenuation for filament densities less than $44.1x10^{2}$/meter, with a particularly interesting analytical result of complete wave transmission with no attenuation at a filament density of $44.1x10^{2}$/meter. Experimentally obtained data appear to negate the validity of this analytical model.

As an alternate formulation, a model based upon the scattering of acoustic waves around a cylindrical body in air was used. For analysis purposes, each filament was assumed to act as a separate cylindrical body with the attenuation evaluated by assuming that the energy scattered by each filament

was irrecoverable. It should be emphasized that this model does not account for interaction effects between adjacent filaments. Attenuation values calculated using this model are low by several orders of magnitude and are not shown. However, a trend is indicated and additional study in the area may be warranted.

Finally, in order to assess the influence of several lamina placed intermittently in a bar specimen, a test specimen with three equally spaced lamina of filament density 18.9×10^{2}/meter was fabricated. Tables II, III, and IV give the results obtained from these tests; Table IV also gives the average lamina attenuation δ for this specimen. It appears that, for the lamina spacing used, this value is approximately the same as the lamina attenuation of a 18.9×10^{2}/meter interface in a specimen with a single lamina of this filament density.

2.3 Wave Propagation in Continuous Filament Rods

To extend the single interface results obtained, multiple layered transverse rods have been fabricated for wave propagation studies in addition to the longitudinal rod studies reported on in Reference 2. Such geometrical influences as wire size and volume percent of filaments has been examined.

2.3.1 Fabrication Process

A description of the fabrication processes involved in producing longitudinal filament bar specimens has been discussed in Reference 2. In all, five long bar specimens were fabricated with wire size, volume fraction of filaments, and center-to-center spacing of wires summarized in Table V.

TABLE V. INTERFIBER SPACING OF LONG BAR SPECIMENS

Wire Diameter (meters)	Volume Fraction (meters)		
	10%	25%	40%
0.04×10^{-2}	0.11×10^{-2}	0.07×10^{-2}	0.05×10^{-2}
0.02×10^{-2}	0.05×10^{-2}	0.03×10^{-2}	

A soft type 304 stainless steel was used as the filament material in all bar specimens, and each bar was machined to nominal dimensions of 1.02×10^{-2} meters in diameter and 76.20×10^{-2} meters in length.

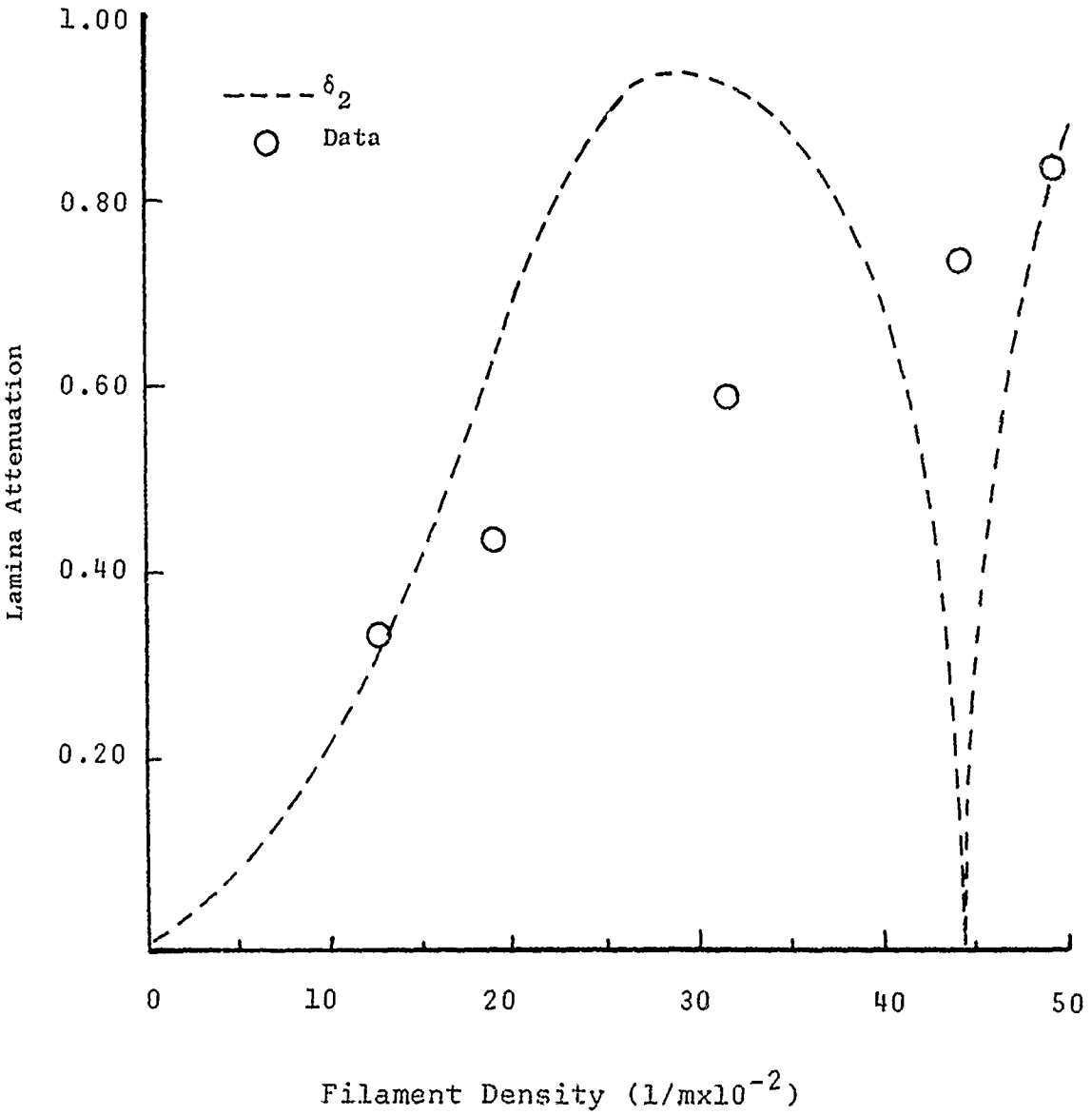

Figure 10. Lamina Attenuation Versus Filament Density

Long bar specimens with filaments oriented in the transverse direction and using the same wire material as the longitudinal bars were also fabricated. In all, four composite bar specimens were fabricated duplicating the wire size and volume fraction used in the longitudinal filament specimens with the exception of the 25 , 0.02×10^{-2} meter diameter specimen. Each of the bars was fabricated by using a modification of the winding assembly described in Reference 1, and is shown in Figure 11. In essence, this procedure utilized an enlarged mandrel assembly from which both long bar and penetrator type specimens could be machined. The wires were accurately spaced by means of a rotating threaded shaft. Control of inter-layer spacing was insured by use of prepared shim stock. After winding, the entire mandrel assembly was cleaned several times in a trichloroethylene vapor degreaser. A matrix composition of Epon 828 epoxy resin mixed with 12 parts per hundred of Curing Agent D was then poured on the mandrel assembly and furnace cured for two hours at 65.6°C.

After curing, the composite was separated from the mandrel so as to produce two rectangular blocks approximately 1.27×10^{-2} meters x 7.63×10^{-2} meters x 30.5×10^{-2} meters in size. Specimens of desired shape were then produced from these blocks, including both transverse and off-angle bar specimens as well as transverse and longitudinal filament penetrator specimens. In the general machining process, it was necessary to rough cut the specimens from the block using a water-cooled friction saw before grinding the specimens to the final desired dimensions. The transverse filament bar specimens were machined to the nominal dimensions of 0.89×10^{-2} meter square by 30.5×10^{-2} meters in length. A summary of several of the axial and transverse specimens fabricated are shown in Figure 12.

2.3.2 Experimental Procedure

In order to monitor the impact-generated waves, foil resistance gages were used to record the strain in the bars. Two BLH-FAE-06J-1256 foil gages were bonded to the surface of each bar using Eastman 910 adhesive. These gages were located near the impact end and center of the bar specimens, and each gage formed one leg of a Wheatstone bridge circuit described in the test procedures section for single transverse lamina bars.

The test procedures used for these bar specimens were identical to those used for the bars having a single transverse lamina and are shown in Figure 4. As in the preceding experiments, the strain gage output was displayed on an oscilloscope and recorded photographically. Typical recorded strain pulses in each bar and the first wave reflections showing the change in initial wave shapes are shown in Figure 13. In addition, Figure 14 shows multiple reflection in each bar and illustrates how the pulse is attenuated through the material.

The axial reinforced bar specimens of circular cross-section were tested using the air gun assembly, as shown schematically in Figure 15.

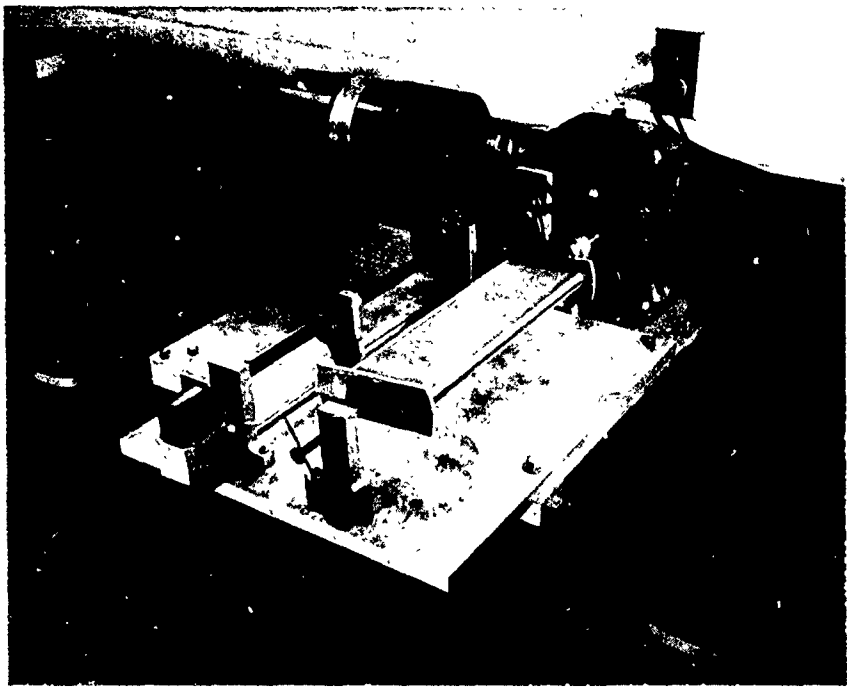

Figure 11. Transverse Long Bar Winding Assembly

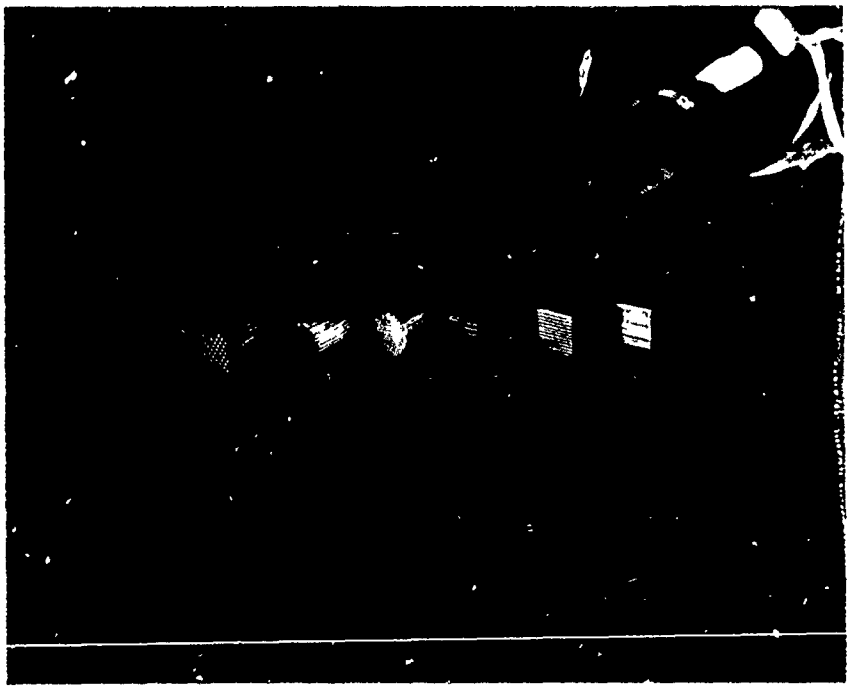

Figure 12. Axial and Transverse Bar Specimens

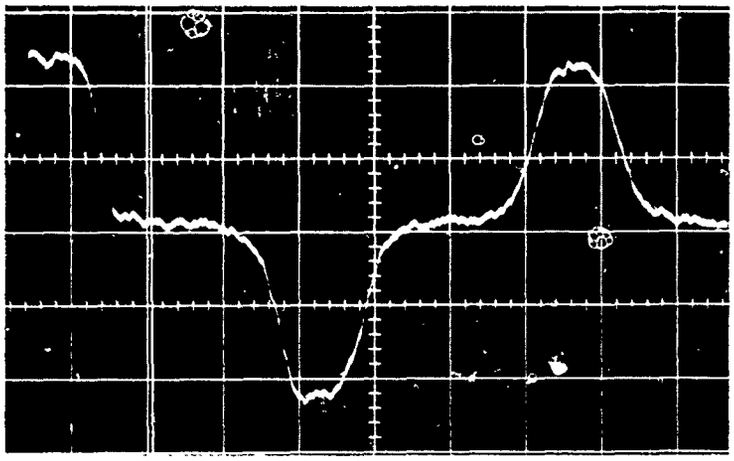

(a) 10%, 0.0203×10^{-2} m

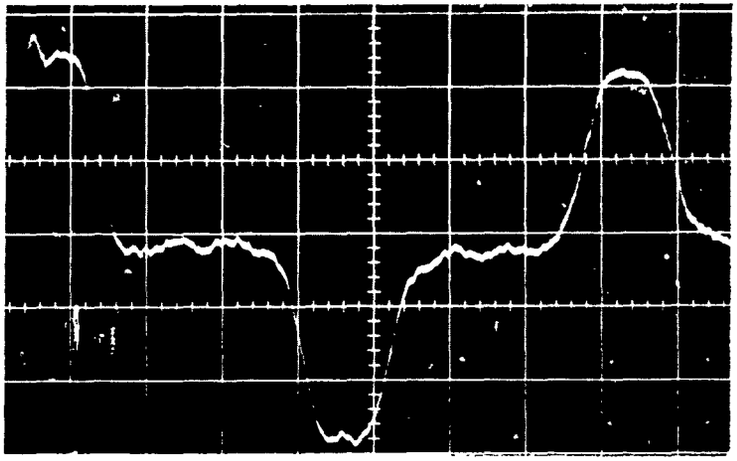

(b) 10%, 0.0406×10^{-2} m

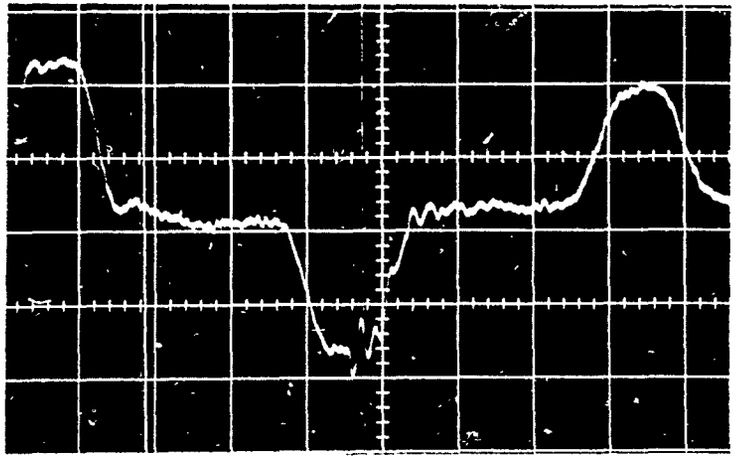

(c) 25%, 0.0406×10^{-2} m

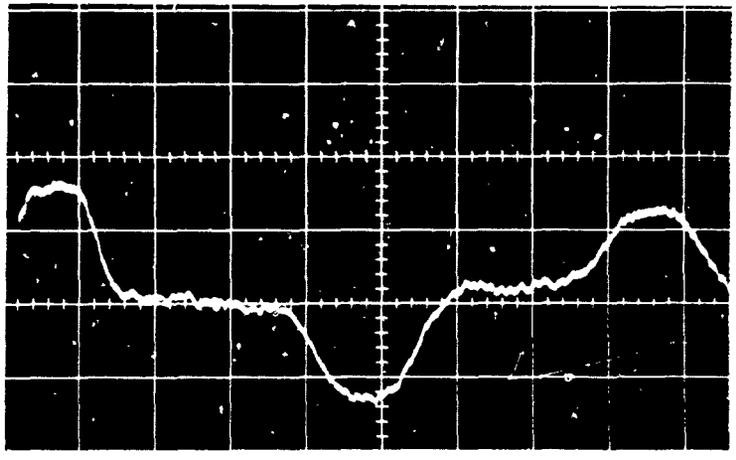

(d) 40%, 0.0406×10^{-2} m

Figure 13. Initial Wave Pulses in Transverse Filament Bar Specimens

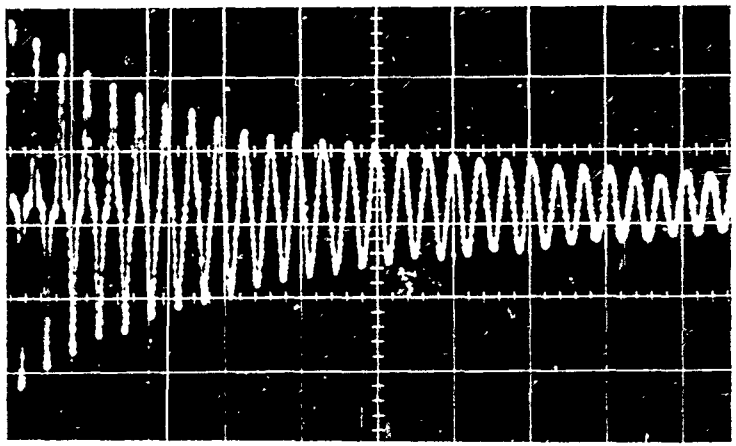

(a) 10%, 0.0203×10^{-2} m

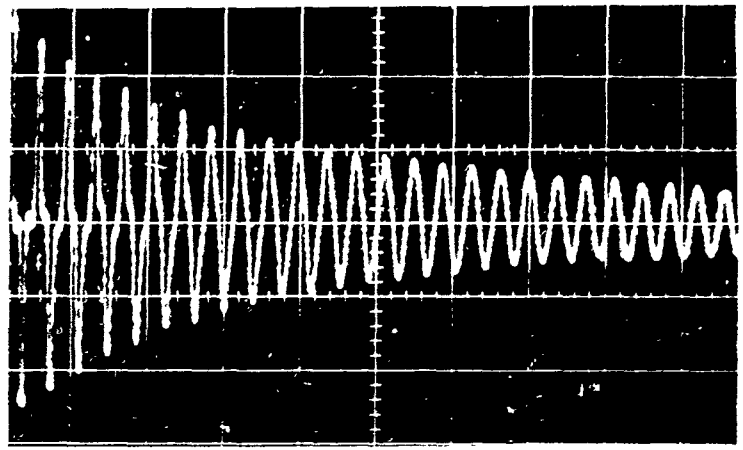

(b) 10%, 0.0406×10^{-2} m

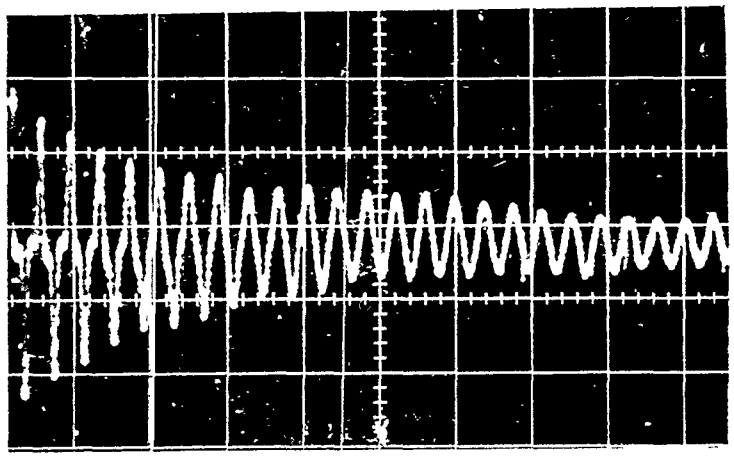

(c) 25%, 0.0406×10^{-2} m

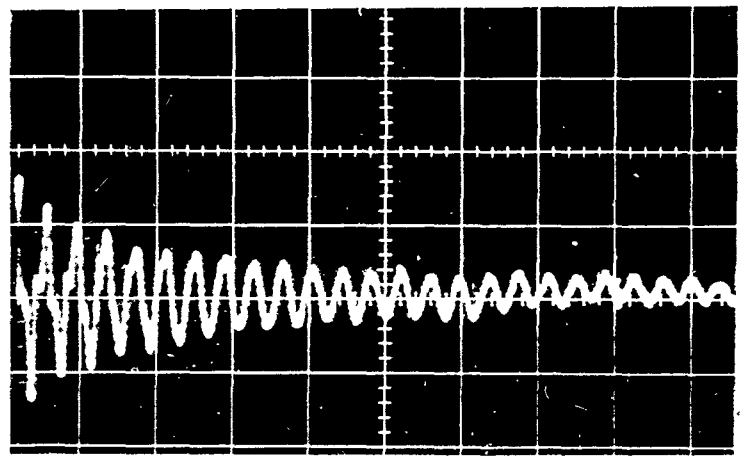

(d) 40%, 0.0406×10^{-2} m

Figure 14. Multiple Reflection Pulses in Transverse Filament Bar Specimens

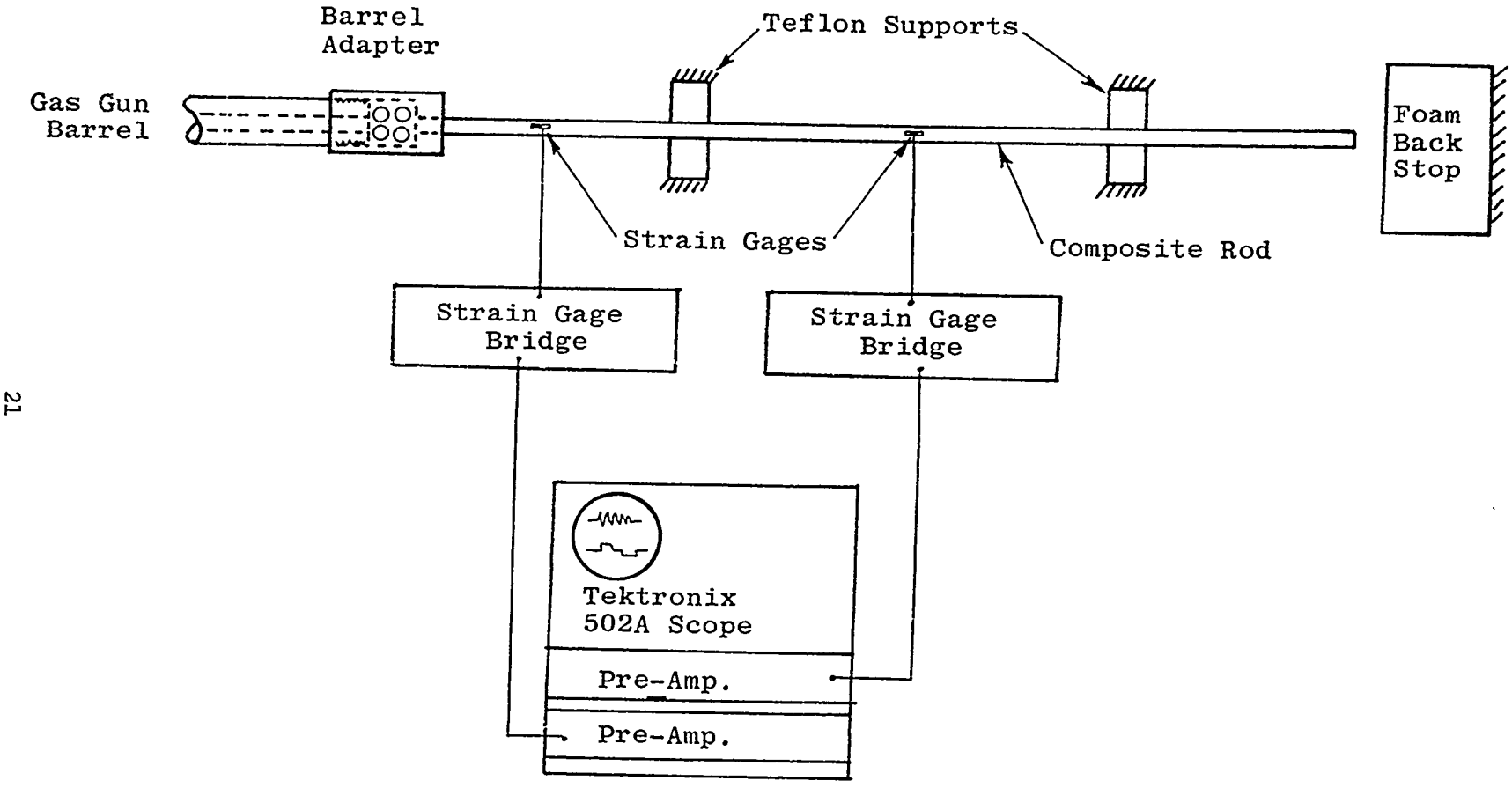

Figure 15. Test Apparatus Schematic for Impact of Axially Reinforced Bars

An epoxy impactor was fired from the air gun at low speeds to produce strain pulses in each bar. Details of the testing procedure and typical photographs of the initial and multiple reflected wave forms obtained are contained in Reference 2.

2.3.3 Wave Speeds, Amplitude Attenuation, and Dispersion

These tests were conducted to examine how one-dimensional waves are propagated in longitudinal and transverse filament-type specimens considering the influence of such geometrical effects as wire size, spacing, and number of filaments. In addition, the change in wave shape and amplitude has been examined for the various specimens tested.

The speed with which a strain pulse propagates through a composite bar can be determined from the pulse reflection figures by direct measurement.

A summary of the experimentally determined wave speeds for both the axial and transverse bar specimens is included in Table VI, while Figure 16 summarizes the experimental and analytically predicted wave speeds. The wave speeds have been calculated according to the rule of mixtures using

$$C = \sqrt{E/\rho} \tag{1}$$

where

C = wave speed (m/sec)

E = composite bar modulus $\left(\frac{kg}{m^2}\right)$

ρ = density $\left(\frac{kp}{m^3}\right)$

The axial filament bar modulus has been calculated using the rule of mixtures relationship

$$E_a = E_f V_f + E_m V_m \tag{2}$$

where the subscripts f and m refer to filament and matrix, respectively. The modulus in the transverse direction has been calculated according to Reference 6 as

$$E_t = E_m \frac{(1 + 2\eta V_f)}{(1 - \eta V_f)} \tag{3}$$

where

$$\eta = \frac{(E_f/E_m - 1)}{(E_f/E_m + 2)} .$$

The density has been calculated using the equation

$$\rho = \rho_f V_f + \rho_m V_m . \tag{4}$$

TABLE VI. WAVE SPEEDS IN LONG BAR SPECIMENS

Material	Wave Speed m/sec			
	Axial Reinforcement		Transverse Reinforcement	
	Measured	Predicted	Measured	Predicted
Steel	5010	5010	5010	5010
Epoxy	1867	1910	1867	1910
10%-0.0002	3607	3620	1168	1593
26%-0.0002	4534	4343	*	*
10%-0.0004	3754	3546	1618	1593
26%-0.0004	4547	4252	1550	1504
40%-0.0004	4910	4650	1550	1542

*No specimens.

TABLE VII. PULSE ATTENUATION IN LONG BAR SPECIMENS

Material	Attenuation Coefficient (1/m	
	Axial Reinforcement (8.1×10^{-2}m projectile)	Transverse Reinforcement (5.1×10^{-2}m projectile)
Steel	0.010	0.013
Epoxy	0.039	0.051
10%-0.0002	0.031	0.069
26%-0.0002	0.019	*
10%-0.0004	0.032	0.064
26%-0.0004	0.024	0.068
40%-0.0004	0.010	0.073

*No specimens.

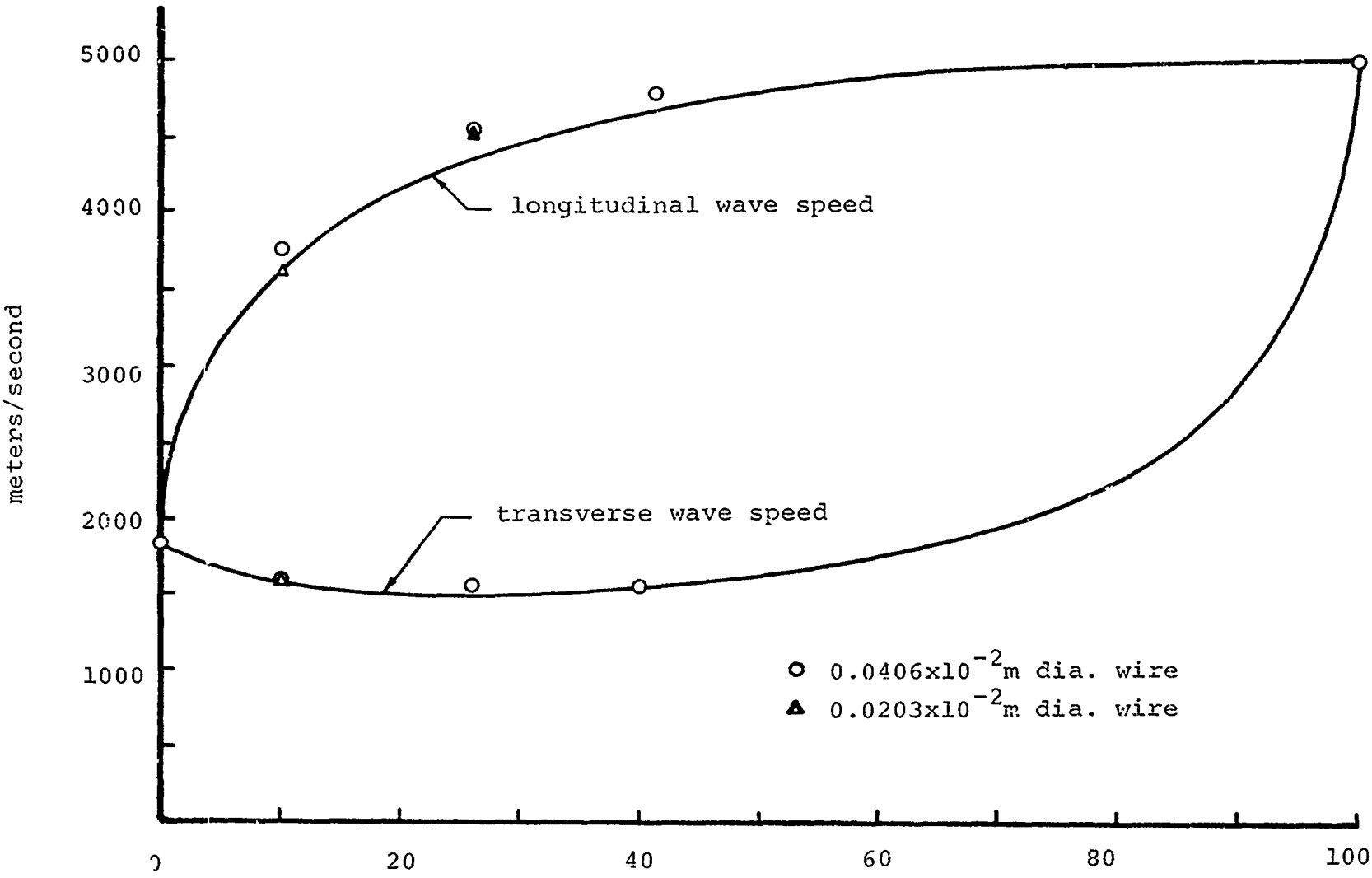

Figure 16. Wave Speed in Axial Filament Specimens

The pulse attenuation for both the transverse and axial filament bar specimens has been measured. A summary of the measured results obtained for both the transverse and axial bar tests is shown in Table VII and graphically in Figures 17 and 18.

The propagation and subsequent attenuation - dispersion of any given initial strain pulse can be predicted using linear viscoelastic theory providing that the material attenuation coefficient α and the pulse velocity C are known as a function of frequency. These quantities have been measured using a Bruel and Kjaer System composed of an Automatic Frequency Response Recorder Type 3329, Complex Modulus Apparatus Type 3930, and Band Pass Filter Set Type 1612. The frequency range of this system is 10,000 cps, and the assembled apparatus is shown in Figure 19.

The experimental procedure consists of exciting a small cantilever specimen of the desired material and observing its response. For calculation, the real part of the complex modulus can be determined from a knowledge of the natural frequencies of the beam. The sharpness of the resonance peak provides a measure of the material damping factor d and phase angle δ between the applied load and deformation, from which the attenuation coefficient can be calculated. Analytically, complex modulus is expressed as

$$E^* = E_1(1 + id) \tag{5}$$

where

E_1 = real part of complex modulus

d = damping factor = tan δ

δ = phase angle between σ and ϵ.

For each natural frequency,

$$E_1 = C/8\pi^2\rho \left(\frac{\ell^2}{h} \cdot \frac{f_n}{k_n} \right)^2 . \tag{6}$$

In the case of small damping, $d \ll 1$, the phase velocity is,

$$C = \sqrt{\frac{E^*}{\rho}} \simeq \sqrt{\frac{E_1}{\rho}} . \tag{7}$$

The attenuation factor is then determined from

$$\alpha = \frac{\pi}{c} df_n . \tag{8}$$

For the higher frequencies, appropriate corrections for shear and rotatory inertia effects are necessary as described, for example, in Reference 15.

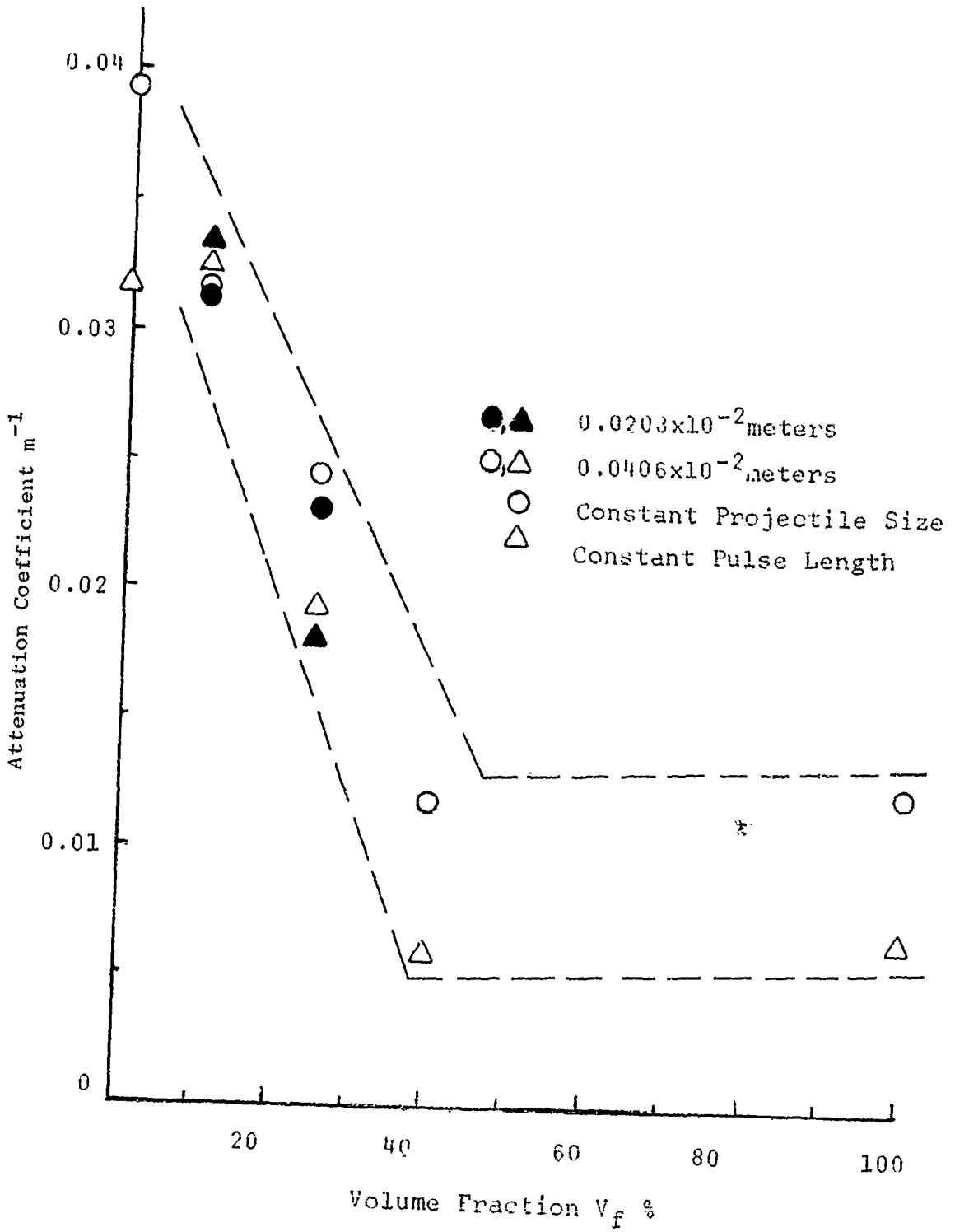

Figure 17. Wave Attenuation in Axial Filament Specimens

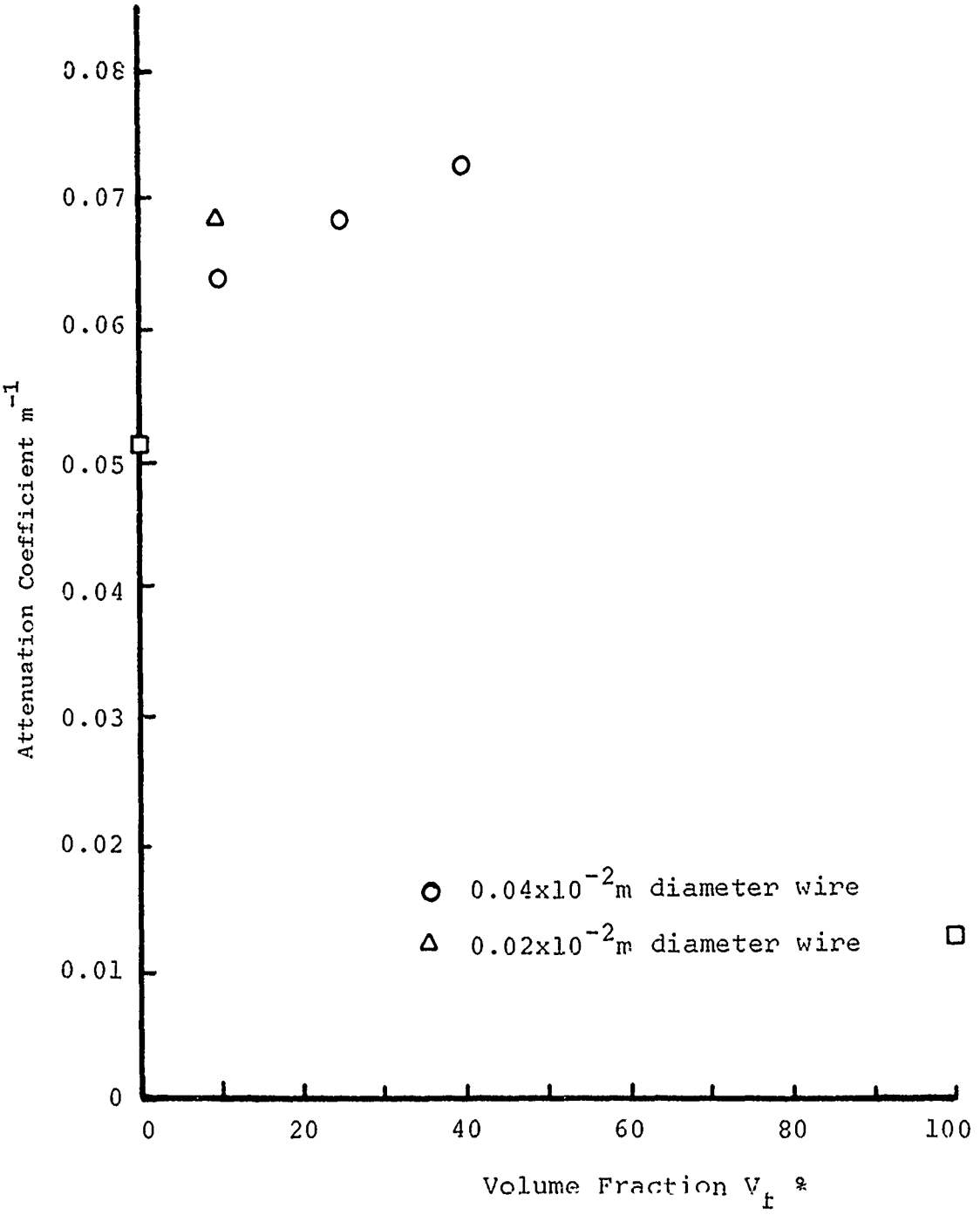

Figure 18. Wave Attenuation in Transverse Filament Specimens

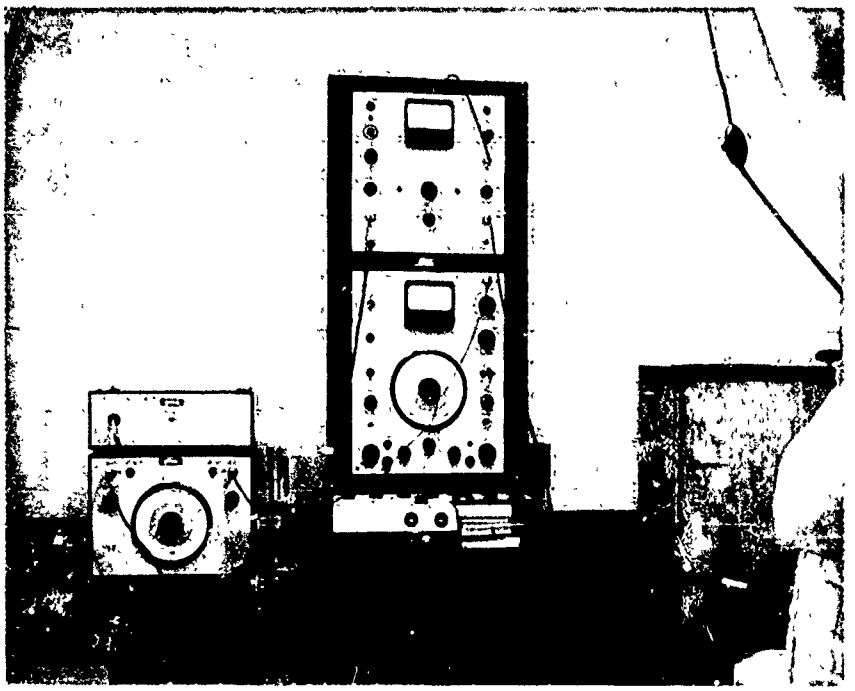

Figure 19. Complex Modulus Test Equipment

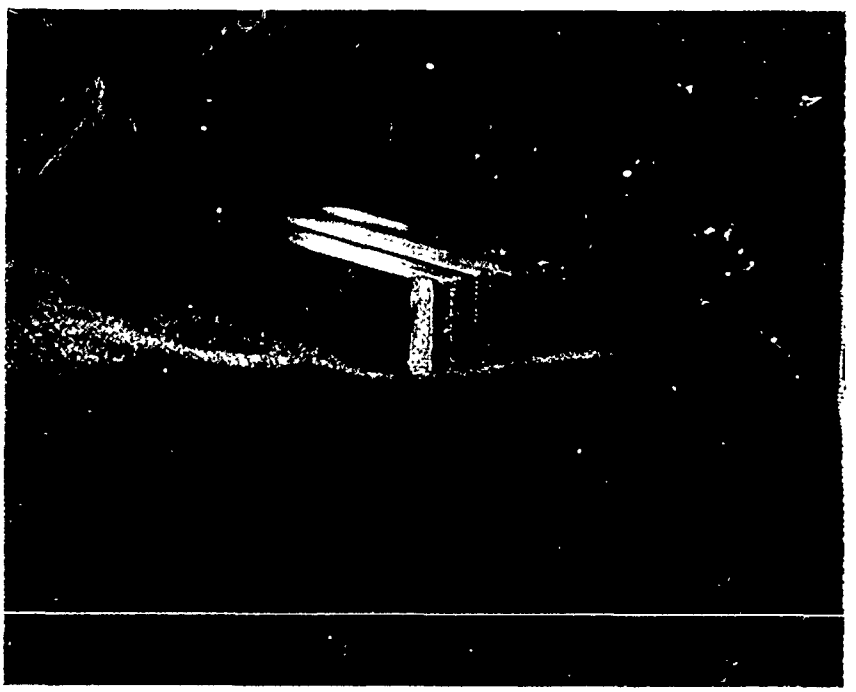

Figure 20. Complex Modulus Test Specimens

To conduct these tests, steel-epoxy small bar specimens with the same wire size and volume percent of filaments as those used in the impact wave study tests were fabricated. These specimens and nominal dimensions of 0.38×10^{-2} x 1.02×10^{-2} x 30.5×10^{-2} meters and are shown in Figure 20. Fabrication procedures were similar to those used for producing the long bar specimens. Typical results obtained from these tests for steel epoxy and composite specimens are shown in Figures 21 and 22. This data can be used directly for calculating the attenuation and dispersion of arbitrary strain pulses in the composite bars. The analytical procedure consists of describing the initial strain pulse in terms of an infinite Fourier integral. The resulting wave equation can then be solved using a Fourier transform technique to give an integral over the frequency range, which may then be evaluated numerically.

The phase velocity at very high frequencies can be measured using an ultrasonic technique which consists of transmitting a short burst of ultrasonic waves through a small material sample and measuring the time of transit. This is accomplished by using two PZT-5 ceramic piezoelectric transducers in the test apparatus shown in Figure 23. One-dimensional waves are introduced into the test specimen by application of a short burst of high-frequency sinusoidal voltage to the transmitting transducer. An identical receiving transducer is then used to display the transmitted wave pulse on an oscilloscope unit. In the present tests a Tektronix Type 549 oscilloscope with a 1A1 dual-trace plug-in unit has been used. The difference in transit times between the transit time of the pulses with and without the specimen can be measured directly from recorded oscilloscope traces, as shown in Figure 24. The upper trace in the figure represents the waves as transmitted through a 0.63×10^{-2} meter aluminum buffer only, while the lower trace shows the waves transmitted through the buffer and specimen together.

The piezoelectric transducers used for the tests were 1.27×10^{-2} meters in diameter and were used in matched sets for frequencies of 1.0, 2.5, 4.0, 5.0, and 10.0 mhz. They were bonded to 1.27×10^{-2} meters diameter epoxy mounts approximately 2.54×10^{-2} meters long. To excite the transducers, a Wavetek model 144 HF Sweep Generator was used to apply short bursts of ten to twenty waves to the transducers, with the delay time between bursts adjusted so that interference between bursts did not occur.

In some cases, a clear wave form could be received due to the attenuation or dispersion in a particular sample, and an individual wave could not be identified. This was especially true at the higher frequencies, and typical results are shown in Figure 25. A summary of the results of all tests are shown in Table VIII.

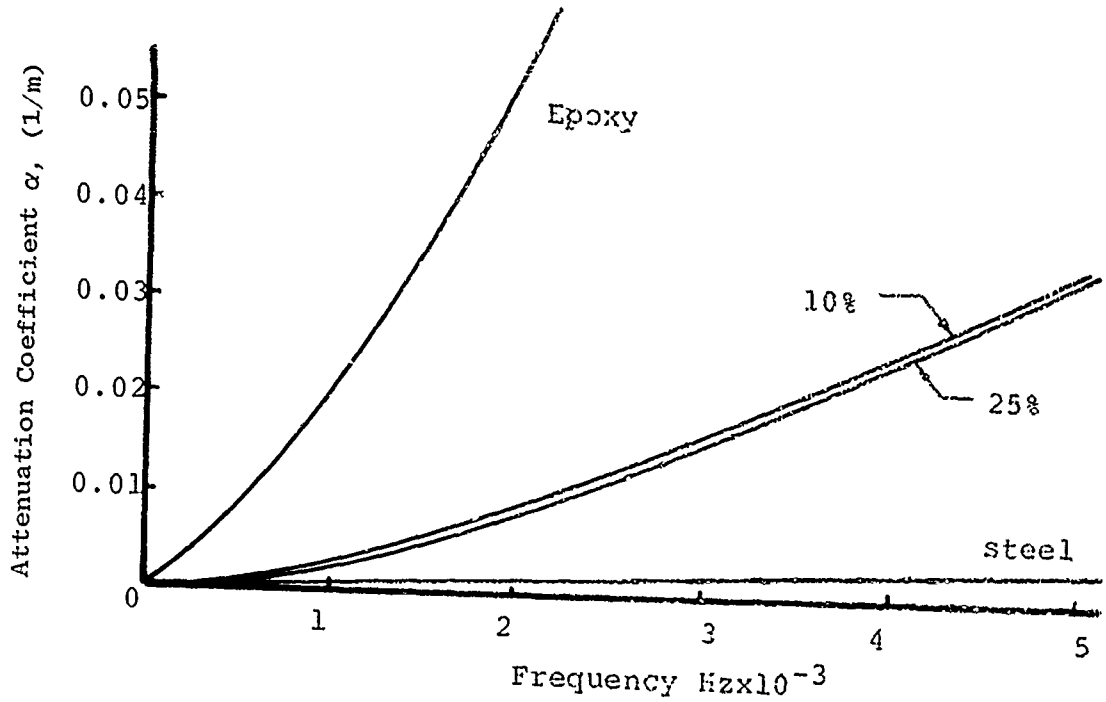

Figure 21. Attenuation Coefficient of Composite Specimens as a Function of Frequency 0.0203×10^{-2}m Wire Diameter

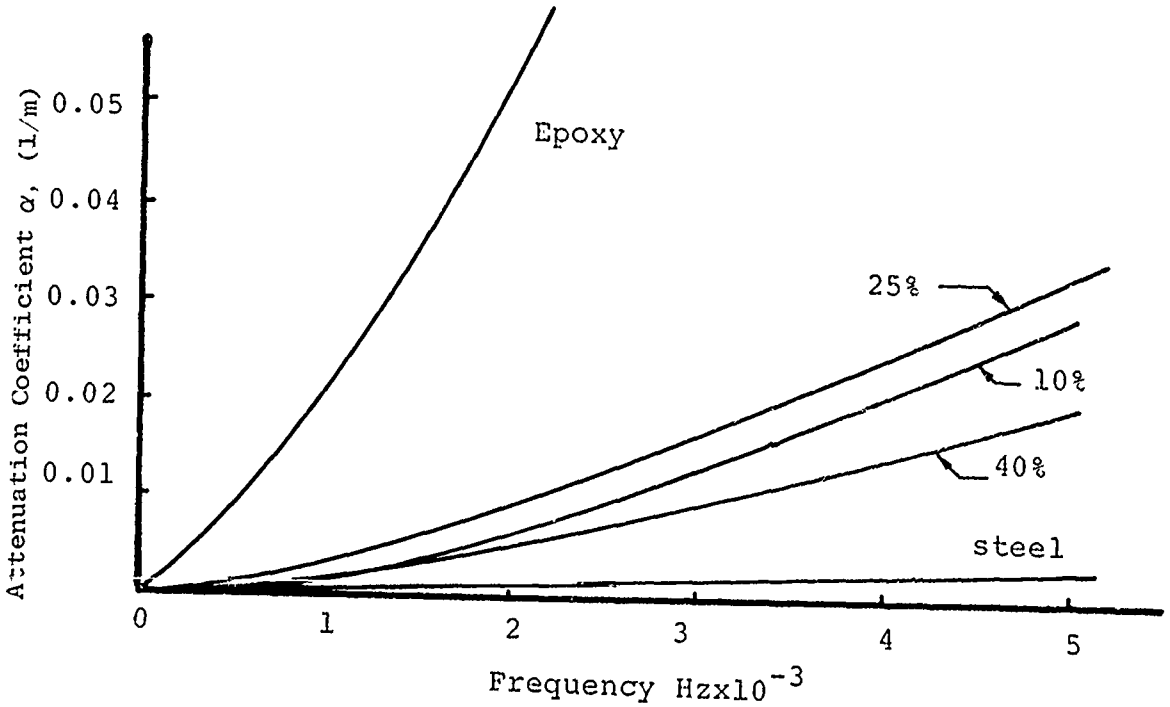

Figure 22. Attenuation Coefficient of Composite Specimens as a Function of Frequency 0.0406×10^{-2}m Wire Diameter

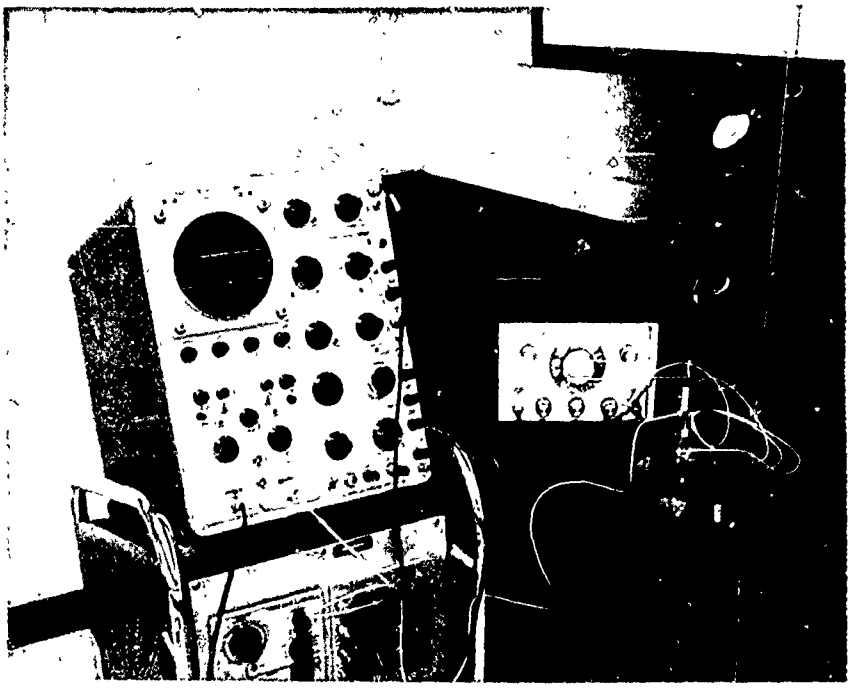

Figure 23. Test Apparatus for Wave Speed Determination at Ultrasonic Frequencies

2.4 Impact Failure of Composites

Various types of compressive failure modes have been observed for composite materials of varying geometries at both low and high strain rates [16]. Of particular interest are the impact fracture characteristics associated with specimen geometry, as shown in Figure 26. Since the controlled composite geometry specimens, as impacted, produced distinct fracture patterns of various segmented arrays, an examination of the basis for these fractures was pursued. This phase of the investigation was then directed to studying the effect of impact loads on long bar specimens, the wave propagation effects, and resultant fracture. The first long bar fracture experiments have been conducted on pure circular diameter epoxy bars of nominal dimensions 0.1×10^{-2} meters diameter x 20×10^{-2} meters impacted by epoxy cylindrical specimens at 0.1×10^{-2} meter diameter x 6.4×10^{-2} meters. The test equipment used for this study has been described in References 1 and 2. As can be seen from Figure 27, a reflected tensile wave at the free end of the long bar produced fracture at an equivalent length of the impactor. It has been further observed that failure could be initiated within the impacted bar specimens at specific locations by introducing a local stress raiser. For some of the epoxy long bars tested, this was accomplished indirectly by mounting procedures to accommodate wire resistance strain gages to monitor the impact pulses. The various composite bar specimens described in the above sections were considered for impact failure tests; since the

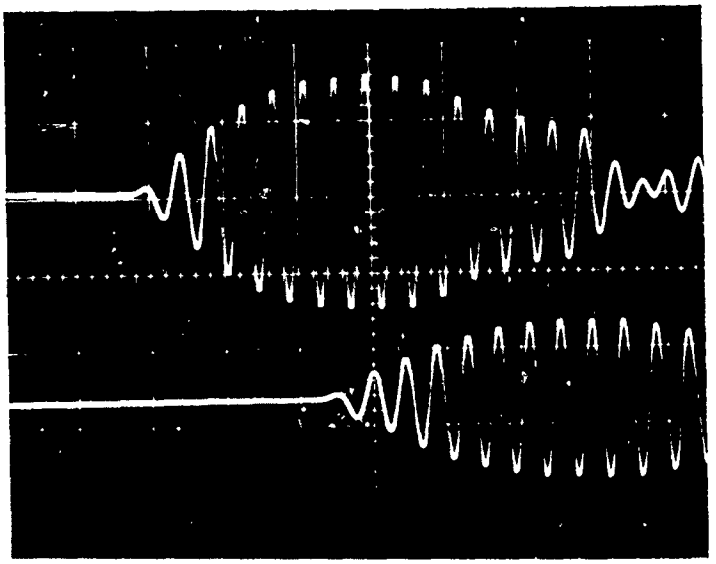

Figure 24. Typical Oscilloscope Record of Ultrasonic Pulse Transmission

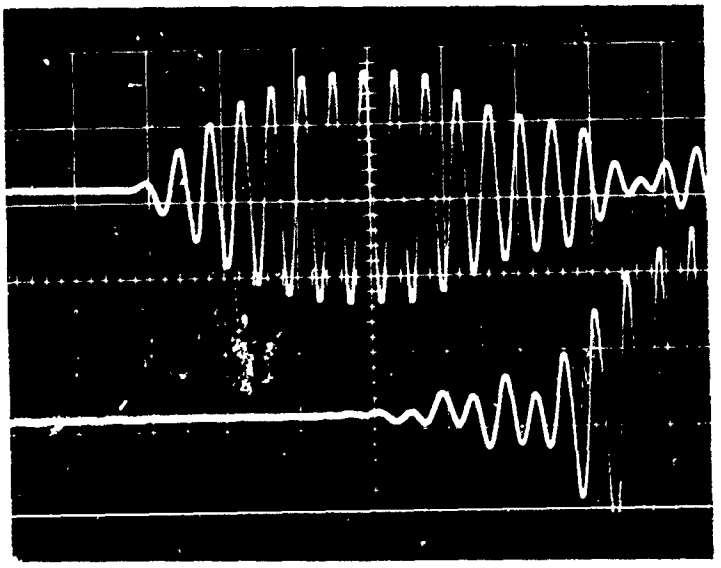

Figure 25. Typical Oscilloscope Record of Ultrasonic Pulse with Severe Attenuation and Dispersion

TABLE VIII. PHASE VELOCITY DATA

(a) Wave Speed in Constituent Materials (meters/sec)

Material	Frequency - Mhz				
	1.0	2.5	3.9	5.0	9.5
Steel	5400	5290	5400	5400	5340
Epoxy	1860	1880	1900	*	*

(b) Wave Speed in Composite Materials (meters/sec)

Frequency (mhz)	Wire Diameter ($mx10^2$)	Volume Fraction - %		
		10	26	40
1.0	0.01	2520	3330	3480
	0.02	2660	3510	3610
	0.04	2720	3100	4040
2.5	0.01	4180	3890	4140
	0.02	2970	3780	3860
	0.04	2460	3180	3330
3.9	0.01	4270	4170	4290
	0.02	4370	*	3910
	0.04	*	3150	3350
5.0	0.01	3850	*	3400
	0.02	*	*	*
	0.04	*	*	3400

*Indicates transmitted wave was too attenuated and/or dispersed to obtain an accurate wave speed measurement.

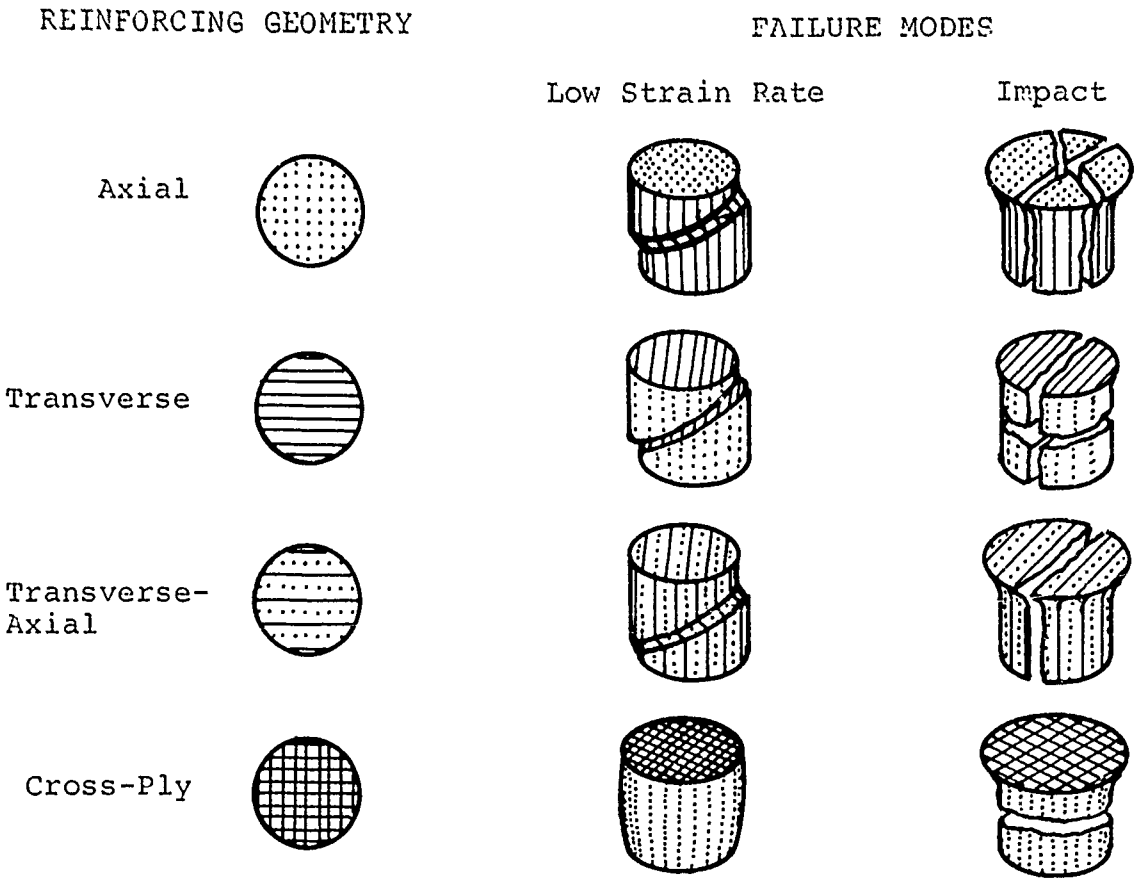

Figure 26. Compressive Failure Modes for Composite Materials

fabrication process required to produce such specimens was lengthy and the necessity for repetition of wave speed, attenuation, and dispersion tests considered essential, the structural integrity of these specimens was unaltered. Based on the small specimen impact data and the failure obtained from impacted long bar epoxy specimens, it appears that fracture control for transverse filament composites is feasible, and that other geometrical configurations can be designed to fracture at specified locations by locating crack raisers on the specimen. Established experimental priorities precluded an extensive examination of crack-induced failure phenomena.

2.5 Conclusions

In the present investigation the propagation of small amplitude pulses have been examined in long bar specimens with varying wire size and fiber orientation. Some conclusions which can be drawn from this work are:

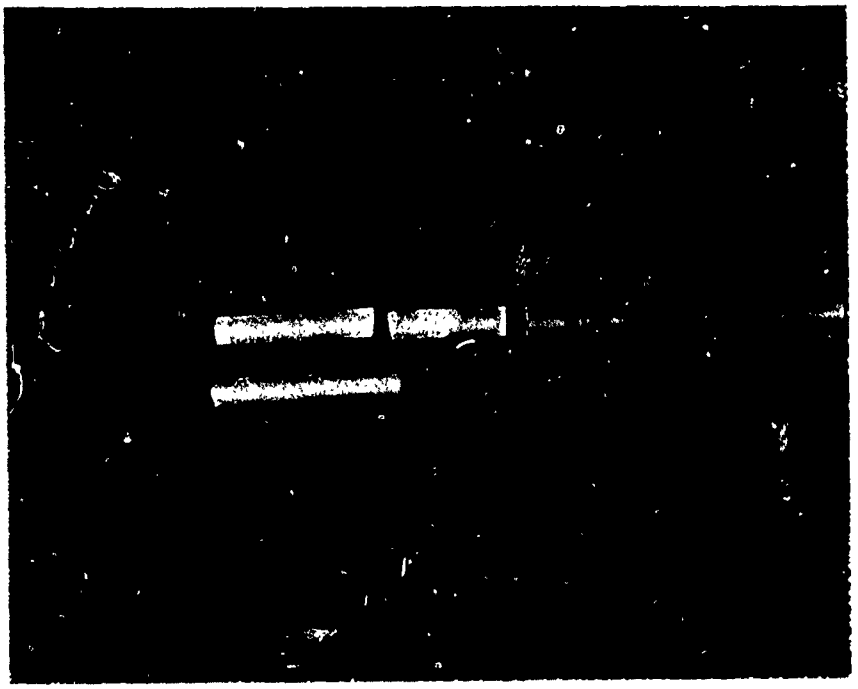

Figure 27. Impact Failure of Epoxy Rods

(1) Wave speeds in unidirectional composite bars having filaments either parallel or perpendicular to the bar axis can be accurately predicted using the familiar one-dimensional wave equation for homogeneous materials $c_i = \sqrt{E_i/\rho}$, where ρ is the composite density and E_i is the composite modulus in the direction of the bar axis.

(2) A single composite lamina, located in an otherwise homogeneous medium, provides measurable pulse amplitude attenuation in comparison to a homogeneous media, the effect increasing with increasing filament density.

(3) Linear scaling of single lamina attenuation results appears to provide favorable agreement with experimental attenuation found in specimens with widely spaced single lamina.

(4) For longitudinally reinforced composite bars, the value of the attenuation coefficient for strain pulses lies between the values of the attenuation coefficients for each of the constituent materials. However, for a transversely reinforced bar, the attenuation in the composite bar exceeds that of either of the constituent materials for the range of volume fractions tested.

(The reverse of this page is blank.)

SECTION III

PLATE IMPACT STUDIES

3.1 Introduction

Information generated from the wave propagation studies described above focuses attention on the importance of pulse behavior on the resultant location and nature of the fracture phenomenon. The second phase of this investigation has been directed toward control of penetration and fracture characteristics of composite specimens impacting rigid and plate type targets. This phase of the investigation is directed toward identification and description of composite parameters necessary to allow prediction and control of nature, location, and timing of fracture of projected specimens during impact and trajectory of fractured segments. Further, the data obtained is directly applicable for comparison with analytical data generated from terminal ballistics computer codes.

3.2 Plate Penetration Studies

The feasibility of fabricating composite plate specimens has been reported in Reference 2. In order to investigate the failure/fracture and energy-absorbing characteristics of such specimens, a series of terminal ballistics tests has been conducted. In these tests, blunt-ended steel projectiles of diameter 0.970×10^{-2} meter and length 2.54×10^{-2} meters have been fired at various composite target materials. Included among the plate materials studies were reference steel plates and such composites as steel-epoxy, fiberglass-epoxy, and various ceramic laminates. Information on the steel plate and impactor specimens are included in Table IX, and a more detailed discussion of the composite plates tested is included in the following paragraphs.

TABLE IX. STEEL PLATE IMPACT DATA

Material	Rockwell Hardness	Dimensions (10^{-2})(meters)	Weight	Penetration Velocity
Steel Plate	B38	15.25 x 15.25 x 0.16	0.286 kg	115 m/sec
Steel Plate	B64	15.25 x 15.25 x 0.32	0.567 kg	224 m/sec
Projectile	B60	0.97 dia. x 2.54	0.015 kg	

3.2.1 Steel-Epoxy

A series of impact tests were run on six steel-epoxy plates of the type described in Reference 2. For all impact tests run, the gas gun previously described in Reference 1 was used. In addition, a special plate-holding fixture, target shield, and related monitoring equipment were assembled. The test setup used is shown in Figure 28. A blunt-ended projectile of the type indicated in Table IX was used as the penetrator. All composite impact tests were run at a constant velocity, this being the required velocity to penetrate a 0.16×10^{-2} meter thick steel plate.

Plate fabrication was accomplished by modifying the winding assembly described in Reference 1. The winding procedure used was similar to that followed for fabricating the transverse bar specimens with the exception of the mandrel used.

All specimens were of the alternating layer type (cross ply) with three basic lay-up types prepared. The various combinations of specimens fabricated and tested are included in Table X. Typical fabricated plate specimens are shown in Figure 29.

TABLE X. STEEL EPOXY PLATE SPECIMENS TESTED

Plate	Weight (kg)	Dimensions (meters x 10^{-2})	Density kg/m^3	Fiber Lay-up
1	0.18	15.25 x 15.25 x 0.43	1813.03	7 ply alternating
2	0.18	15.25 x 15.25 x 0.43	1813.03	7 ply alternating
3	0.26	15.25 x 15.25 x 0.66	1669.09	8 ply alternating
4	0.22	15.25 x 15.25 x 0.50	1846.24	8 ply alternating
5	0.26	15.25 x 15.25 x 0.61	1829.64	10 ply alternating
6	0.27	15.25 x 15.25 x 0.62	1829.64	10 ply alternating

In order to establish criteria for evaluating the terminal ballistics performance of the composite plates, the critical penetration velocity of steel plates of two thickness sizes was determined. Properties of these plates and the penetrator, including Rockwell hardness number, plate geometry, and weight, are included in Table IX. Using the established steel plate critical velocity, blunt steel specimens were impacted against the steel-epoxy plates.

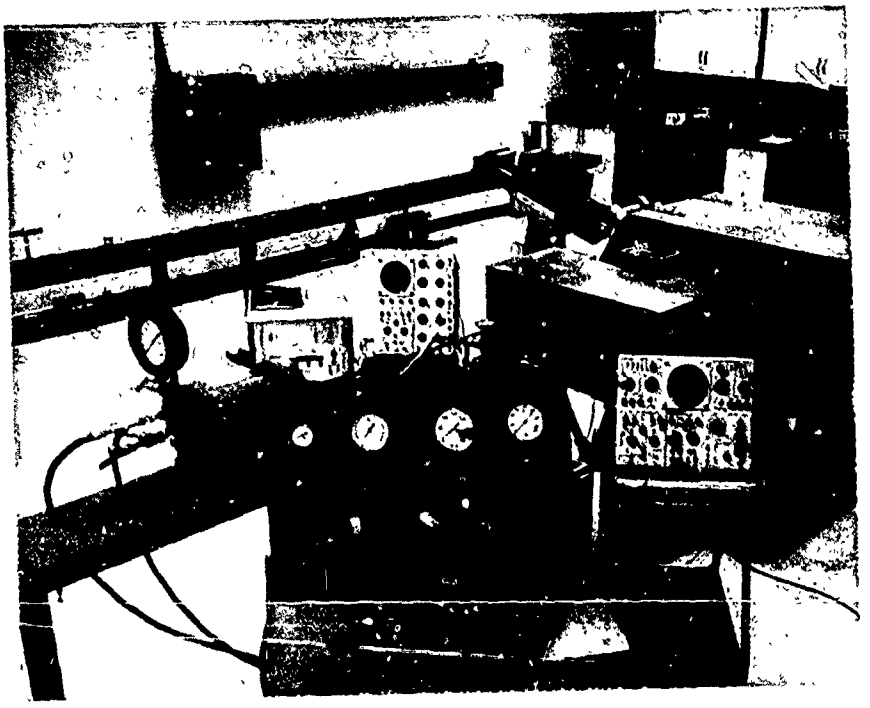

Figure 28. Plate Impact Test Setup

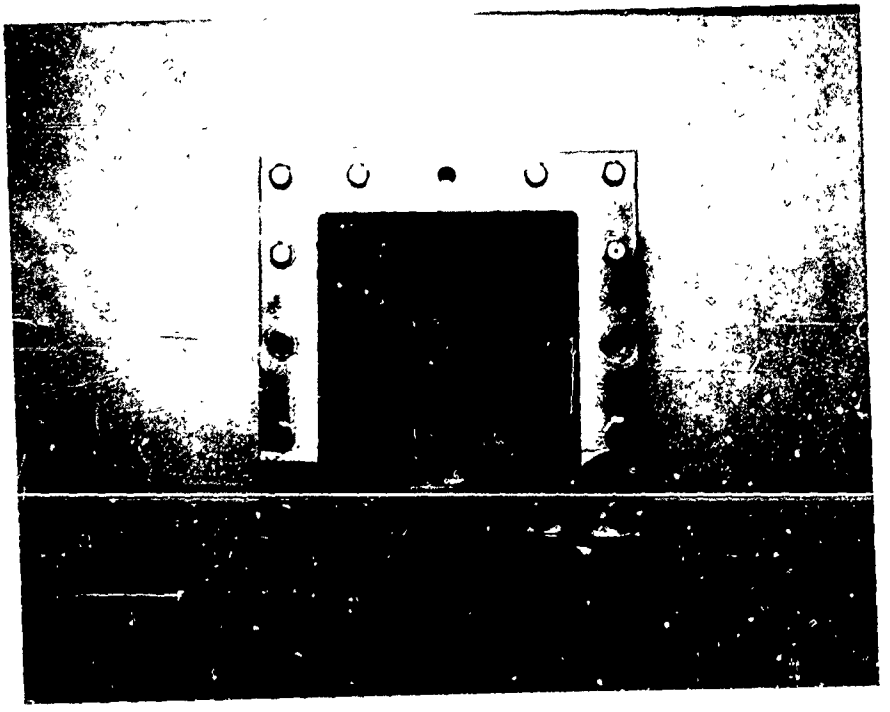

Figure 29. Steel Epoxy Plate Specimens

Results obtained from the impact tests showed that one of the seven- and eight-layer plate specimens were penetrable while one each was not. Further, neither of the ten layer plates was penetrable. The apparent reason that some of the seven- and eight-layer plates were not penetrated may be attributed to the final fabrication process. That is, during the final machining, a small layer of additional epoxy was left on the non-impacted side of the plate, which dispersed the stress wave sufficiently to insure overall structural integrity. A summary of the merit rating of this type composite configuration versus the steel and other composite types is included in Figure 32.

3.2.2 Fiberglass-Epoxy

In the preceding tests the layer arrangement has been staggered in alternating plies to examine the energy-absorbing characteristics of such systems. To investigate the effectiveness of ply arrangement on plate resistance to impact loads, a series of fiberglass epoxy specimens was fabricated. The plates consisted of 15 layers in different combinations of 0° and 90° directions relative to each other. Test procedures consisted of determining the critical velocities for the various ply combinations fabricated.

The process used for fabricating the plates was filament impregnation. The fibers, which were wound on a cylindrical spool, were Owens-Corning Fiberglass Type ECG 456, 4-end precision control roving, with a density of 2540 kg/m^3 and modulus of elasticity of 7.38×10^9 kg/m^2. To fabricate the plate assembly, a mandrel of the type previously described was placed in a lathe and the fiberglass wound directly onto the rotating mandrel at a winding speed of 0.33 rps. The fiberglass spool was mounted on a friction device in order to maintain tension in the filaments during the winding process. Filaments were fed through a pulley attached to the compound of the lathe across the mandrel, the cross feed of the compound being set at 5.5 threads/m$\times 10^{-2}$. This resulted in a center spacing between each of the free end rovings of 0.18×10^{-2} meters. Upon winding one complete layer of fiberglass, that layer was then saturated with an epoxy-curing agent mixture using a paintbrush. This procedure was repeated until the 15 layers of fiberglass was obtained. Then, Mylar sheets were placed on the outer layers of the plates to provide a smooth finish. In addition, plywood sheets were placed on the plates and held in place using C-clamps during cure of the plates. Two plate specimens were obtained from each winding assembly with nominal dimensions of 15.25 x 15.25 x 0.67 meters and an average weight of 289 gms. Typical fiberglass plate specimens are shown in Figure 30.

Since this test sequence was directed toward obtaining information on the effect of ply arrangement during impact, a record of the ply orientation was maintained and is included in Table XI with reference directions included.

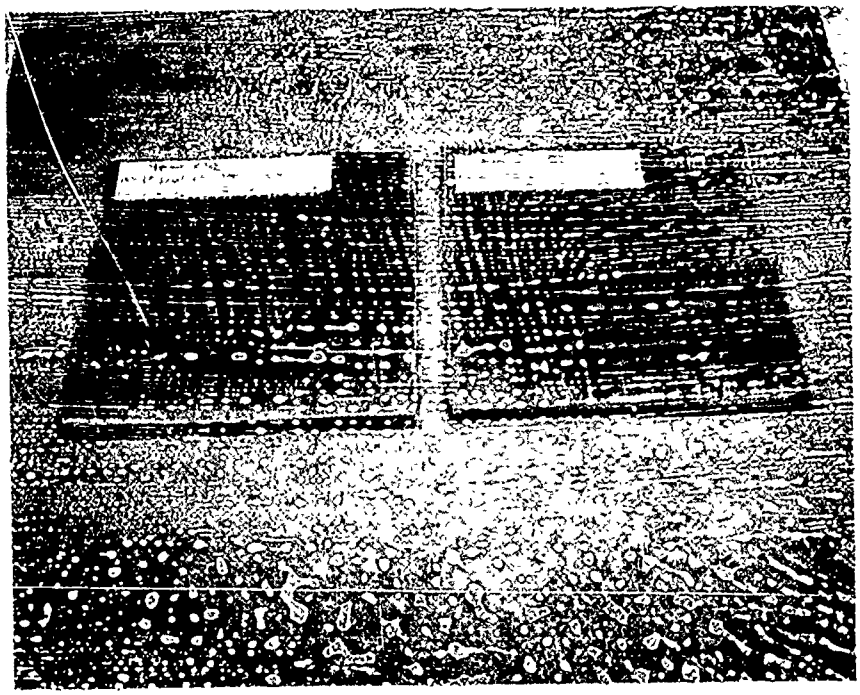

Figure 30. Fiberglass Plate Specimens

TABLE XI. FIBERGLASS COMPOSITE PLATE GEOMETRIES

Plates	Ply Arrangement (layers 1-15)	
1a&b	101010101010101	1 90° 0 (Reference Direction)
2a&b	111000111000111	
3a&b	111110000011111	
4a&b	111111110000000	
5a&b	100111000011111	
6a&b	000000000000000	

The test procedures and projected specimens used were the same as in the steel-epoxy plate tests. Some additional information was obtained, however, on the post-impact velocity of these projected specimens which penetrated the plates. This was accomplished by use of a photochamber containing a stroboscope for illuminating the penetrator at rapid intervals and an open shutter Graflex camera with Polaroid attachment. The time interval between flashes of the strobe and the distance traveled by the projectile as recorded on the film was used as a measure of the penetration velocity. The chamber enclosure was maintained light tight with the shutter of the camera being opened just prior to firing of the penetrator and closed after impact of the back end of the photochamber. A ratio of residual to impact velocity was recorded, with the initial impact velocity selected on the basis of previous data established for fiberglass and recorded in Reference 17.

The plates tested and results obtained are summarized in Table XII. A graphical description of these results is included in Figure 31 and represents on possible plot of the parameters examined.

TABLE XII. FIBERGLASS PLATE IMPACT DATA

Plate	Impact Velocity V_1 (m/sec)	Residual Velocity V_2 (m/sec)
1a	135	0
1b	185	24
2a	165	0
2b	198	69
3a	185	0
3b	198	0
4a	182	0
4b	198	19
5a	185	28
5b	164	0
6a	198	69
6b	159	62

[Figures in parenthesis are plate #]

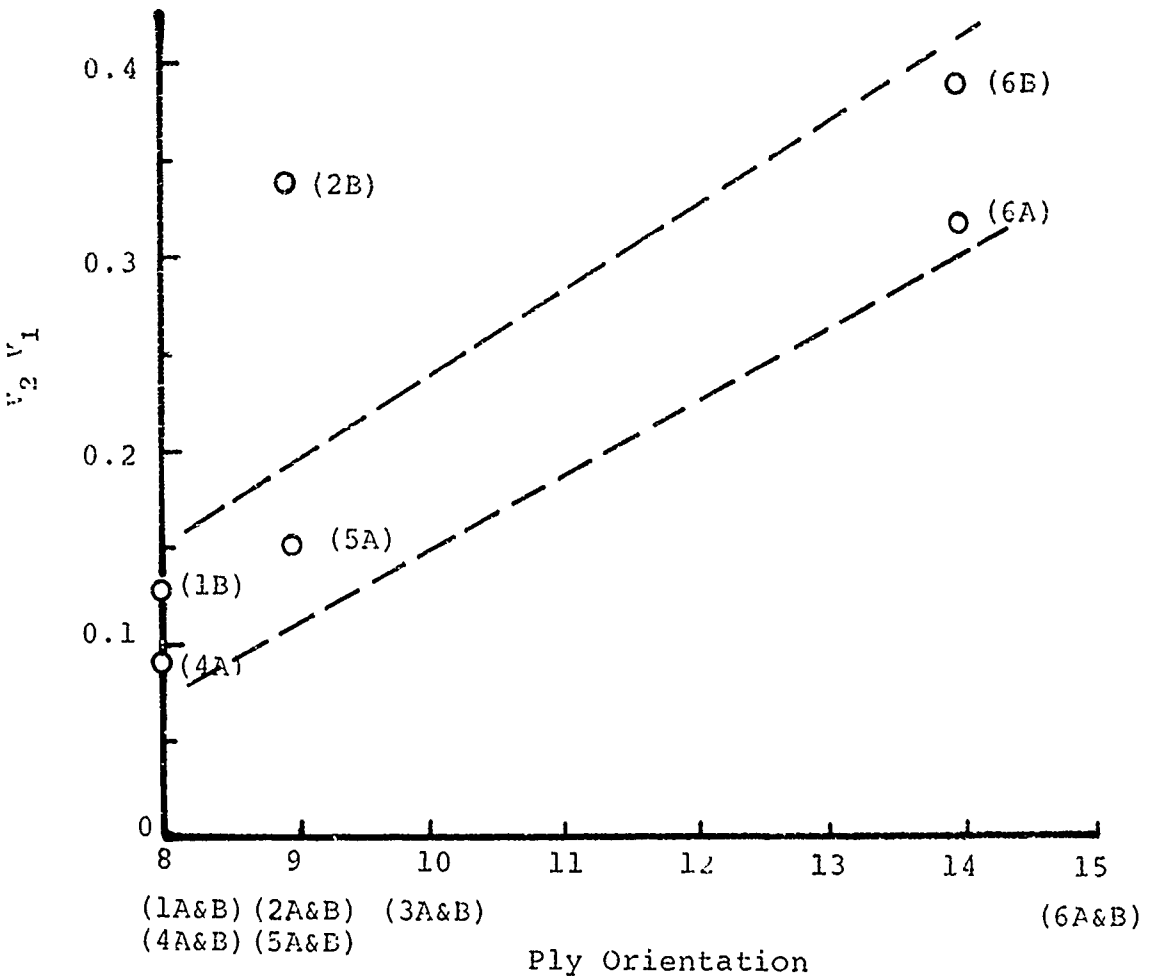

Figure 31. Residual Impact Velocity for Variable Ply Geometry Fiberglass Plates

The ratio of the residual to impact velocity is plotted along the ordinate while the maximum number of layers in the zero to one direction is plotted along the abscissa. Since plates 3a, 3b were not penetrated, no data is available for these systems. A curve representing the assumed relationship between winding combinations and velocity ratios has been indicated on Figure 31. Additional tests are necessary to substantiate this trend.

The dynamic fracture patterns obtained are similar in appearance to stress patterns predicted for static loading of anisotropic plates with cutouts. Photographs of the fracture patterns obtained have been included. It has been further observed that the rate of growth of maximum diagonal distance of the diamond-shaped fracture pattern appears to remain constant through each of the ply orientations. This maximum distance (ΔD) across the fracture patterns appears to be approximately 0.59 meter.

3.2.3 Nylon-Ceramic

In addition to the terminal ballistics tests on oriented fiber composite specimens, a series of tests evaluating layered combinations of nylon-type composites with fiberglass cloth-epoxy backup plates was investigated. It has been pointed out in Reference 18 that hard-faced plate assemblies of ceramic-type materials are effective as energy-absorbers for conical and ojive-type penetrators. Further, it is desirable that the plate materials should be very hard and possess a high compressive ultimate stress and reasonable tensile ultimate stress. The hard face material then serves to blunt the penetrator, and the high tensile stress serves to prevent cracking and breaking of the material under the projectile.

For the present tests the front face nylon and nylon composite plates were furnished by E. I. Dupont while the backup fiberglass cloth plates were fabricated at the contractor laboratory facilities. These plates were composed of 12 fiberglass cloth plies saturated with epoxy resin to produce specimens with a nominal thickness of 0.13 meter. Plates were fabricated using a vacuum bag technique and cured in a circulating oven at 65.5°C. The fabricated fiberglass plates were bonded to the nylon and nylon composites using Pliabond 810 contact cement.

In order to obtain comparative impact test data for this series of tests, a series of plate penetration tests were conducted in order to establish a minimum penetration velocity (critical velocity). This information was generated using a conical-shaped mild steel penetrator with nominal dimensions of 2.86×10^{-2} meters x 0.97×10^{-2} meter in diameter. A critical penetration velocity was established for a single fiberglass plate as well as bonded fiberglass plates. The impact tests conducted on the nylon composite plates bonded to the fiberglass plates were conducted at preselected velocities based on previous tests. A tabulation of these results is given in Table XIII.

TABLE XIII. CERAMIC PLATE IMPACT DATA

Plate	Critical Velocity (mps)	Dimensions (10^{-2}m)	Weight (kg)
Figerblass (1 plate)	67.1	2.92 x 23.6 x 23.6	0.120
Fiberglass (2 plates)	113-122	5.84 x 23.6 x 23.6	0.240
Fiberglass-Nylon	88.5-100.5	6.10 x 23.6 x 23.6	0.200
Fiberglass-Nylon/Alumina	82.4	6.22 x 23.6 x 23.6	0.240
Fiberglass-Nylon/Mica	82.4	6.02 x 23.6 x 23.6	0.235

Based upon the present tests, the nylon composite plate critical velocities are less than the values obtained from the bonded fiberglass plate tests and the nylon-fiberglass plate tests. The nylon composite plates consisted of aluminum-oxide single crystals embedded in the nylon matrix formed by a hot pressing technique. In addition, a micaeous particle-filled nylon plate has been fabricated using similar procedures. The density of crystal packing was of the order of 50 percent with some increase in plate hardness contributed by the particles and a small reduction in tensile strength. The increased plate hardness appears to have little effect on penetrator energy absorption and on blunting the pointed nose of the projectile. It has been discussed in Reference 19 that increased composite densities of the order of 95 percent have been successful in improving plate resistance to penetration.

For comparative purposes, data obtained using blunt and conical penetrators impacted against the various plate specimens have been summarized in Figure 32. The solid curve represents data obtained from penetration tests of a blunted steel cylinder impacting a steel plate and has been used as the reference curve. The steel-epoxy and fiberglass plate tests were impacted by blunt-ended penetrators while the ceramic plate tests utilized conical-type shaped penetrators. A comparison of the various composite plate specimens tested with the reference steel curve shows the relative merit rating of the materials tested. It is noteworthy that the geometrical arrangement of the plies for a fixed number of layers is particularly important in defining a penetration velocity. From the fiberglass specimens tested the best energy-absorbing system was the unsymmetrical ply arrangement associated with plates 3a and 3b.

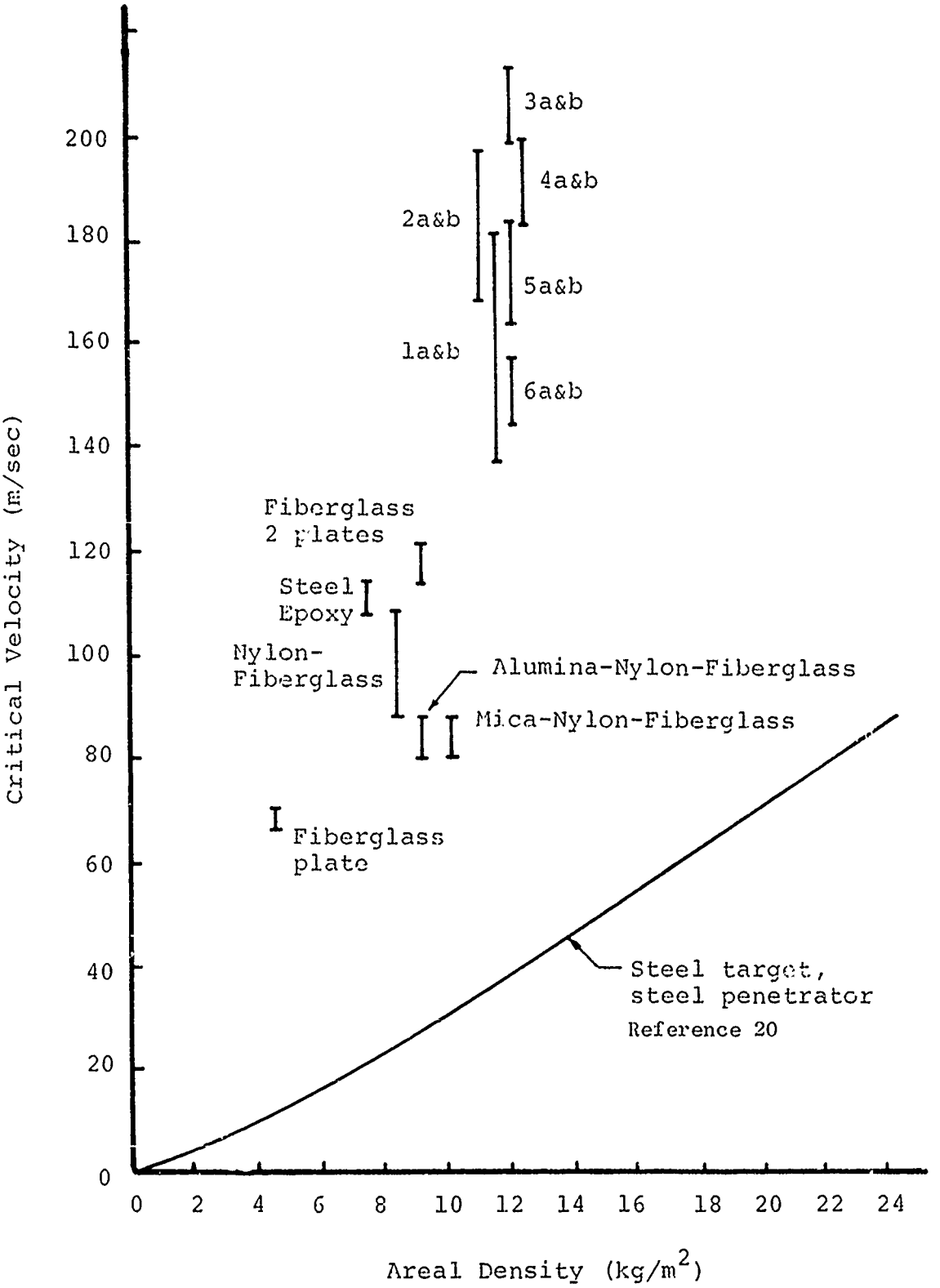

Figure 32. Merit Rating Curve for Plate Impact Tests

3.3 Controlled Fracture of Projected Specimens

The controlled fracture of projected specimens has been examined in a series of impact tests conducted on several target materials. A summary of the types of target materials tested is given in Table XIV.

TABLE XIV. TARGET MATERIALS TESTED

Material	Plate Classification
7075-T6 Al.	Ductile, low mass, high strength
Concrete	Brittle, high mass, low strength
Steel (Cold Rolled)	Ductile, high mass, high strength

The types of projected specimens used in this phase of the test program have been representative of the steel-epoxy model system tested for static and dynamic properties with filaments oriented in the axial and transverse directions. Selection of these particular composite specimens has been based upon basic mechanical properties and wave propagation data accumulated for such composite materials. The aluminum and steel target materials were purchased stock items while the concrete plates were fabricated locally.

Since controlled fracture has been demonstrated on pure epoxy bars subjected to impulsive-type loadings, the controlled fracture of projected-type specimens was anticipated to be feasible. The transverse filament types were considered to be the most susceptible to fracture at some integral multiple of the target plate thickness.

In order to study the controlled fracture characteristics, experiments were carried out using the gas gun, high-speed camera and plate holder as described earlier. In addition, a witness paper backed up with styrofoam was placed at approximately 0.58 meter behind the target to record projectile post-impact patterns. Projectile velocities prior to impact were also recorded in the usual manner. The results of these tests are summarized in Table XV.

The post-impact fracture pattern of axial reinforced specimens impacting on thin metal plates shows a longitudinal breakup or splitting-type failure with a random distribution of the pieces on the witness paper. A typical photograph of the witness paper is shown in Figure 33. The breakup of the projectile as it penetrates is believed to be symmetrical due to a uniform radial expansion and causes a conventional plug-petal failure, as shown in Figure 34.

TABLE XV. CONTROLLED FRACTURE TESTS

Projectile Velocity 382 Meters/Sec, Length 1.27×10^{-2} Meter Unless Specified

Projectile Volume Fracture Percent Wire Diameter Meters x 10^2	Target Thickness Meters x 10^2	Fracture Description (a) Projectile (b) Target (c) Post-Impact Pattern Dimensions in Meters x 10^2
10%-0.04 Axial Reinforced	Aluminum, 0.16	(a) 9-10 pieces 0.97x0.63x0.32; (b) Figure 34; (c) Figure 33
	Concrete, 1.27	(a) Fractured but intact; (b) Shallow crater front face, 2.5 diameter hole, 4.5 diameter spall back side
10%-0.02 Transverse Reinforced	Aluminum, 0.16	(a) Large piece 0.9x1.27x0.63, 6-8 pieces 0.63x0.9x0.32; (b) Figure 42; (c) Figure 35
	Concrete, 1.27	(a) Fractured but intact; (b) Same as concrete above
10%-0.04 Transverse Reinforced	Aluminum, 0.16	(a) Large piece 0.97x0.63x0.32, 8-10 pieces 0.32x3.2x0.16; (b) Figure 34; (c) Figure 35
	Steel, 0.08	(a) Large piece 0.97x0.63x0.63, 3-4 pieces 0.97x0.16x0.16; (b) Figure 43; (c) Figure 36
	Concrete, 1.27	(a) Large piece 0.97x0.63x0.63, 5-6 pieces 0.97x0.32x0.32; (b) Same as concrete above
25%-0.04 Transverse Reinforced	Aluminum, 0.16	(a) Large piece 0.97x0.63x0.16, 5-6 pieces 0.97x0.32x0.32 Many single wires; (b) Figure 42; (c) Figure 37
	Steel, 0.08	(a) Large piece 0.97x0.63x0.63 6-8 pieces 0.97x0.32x0.32; (b) Figure 43; (c) Figure 38
	Concrete, 1.27	(a) Large piece 0.97x0.63x0.63, 5 pieces 0.97x0.63x0.32; (b) Same as concrete above

TABLE XV. CONTROLLED FRACTURE TESTS (CONCLUDED)

Projectile Volume Fracture Percent Wire Diameter Meters x 10^2	Target Thickness Meters x 10^2	Fracture Description (a) Projectile (b) Target (c) Post-Impact Pattern Dimensions in Meters x 10^2
40%-0.04 Transverse Reinforced	Aluminum, 0.16	(a) 6-8 pieces 0.97x0.32x0.32, many single wires; (b) Figure 42; (c) Figure 39
	Steel, 0.08	(a) 3-5 pieces 0.97x0.63x0.32; (b) Figure 43; (c) Figure 40
	Concerte, 1.27	(a) 2 pieces 0.97x0.63x0.32, 4-5 pieces 0.07x0.32x0.32; (b) Shallow crater front face, 2.5 diameter hole, 4.5 diameter spall back side
40%-0.04 Transverse Reinforced Length, 1.9	Aluminum, 0.16	(a) Large piece 0.97x0.97x0.32, 2 pieces 0.97x0.75x0.32; (b) Figure 42; (c) Figure 39
	Steel, 0.08	(a) Large piece 0.97 diameter x 0.97, 4-5 pieces 0.97x 0.75x0.32; (b) Figure 43; (c) Figure 40

The fracture of the lower volume fraction transverse specimens (10 percent filament) was found to be similar to the axial reinforced projectilves in that a random type post-impact pattern resulted after impact with thin metal plates. The post-impact pattern for a 0.0016-meter-thick aluminum plate is shown in Figure 35, and the pattern for penetration of a 0.0008-meter-thick steel plate (same projectile velocity is shown in Figure 36. The fractured particles of the 10 percent transverse reinforced specimens consisted of a rather large piece, eight to ten smaller pieces, and many single filaments while the axial reinforced projectiles resulte in nine to ten almost equal size pieces and single filaments.

Post-impact patterns of the 25 percent transverse reinforced specimens were found to be quite different from those of the axial reinforced and 10 percent transverse reinforced projectiles. In this case the post-impact pattern is slightly elongated, as shown in Figure 37, for impact with an aluminum plate and in Figure 38 for impact with a steel plate. The complete understanding of this elongated post-impact pattern was not apparent until tests were performed using 40 percent transverse reinforced specimens.

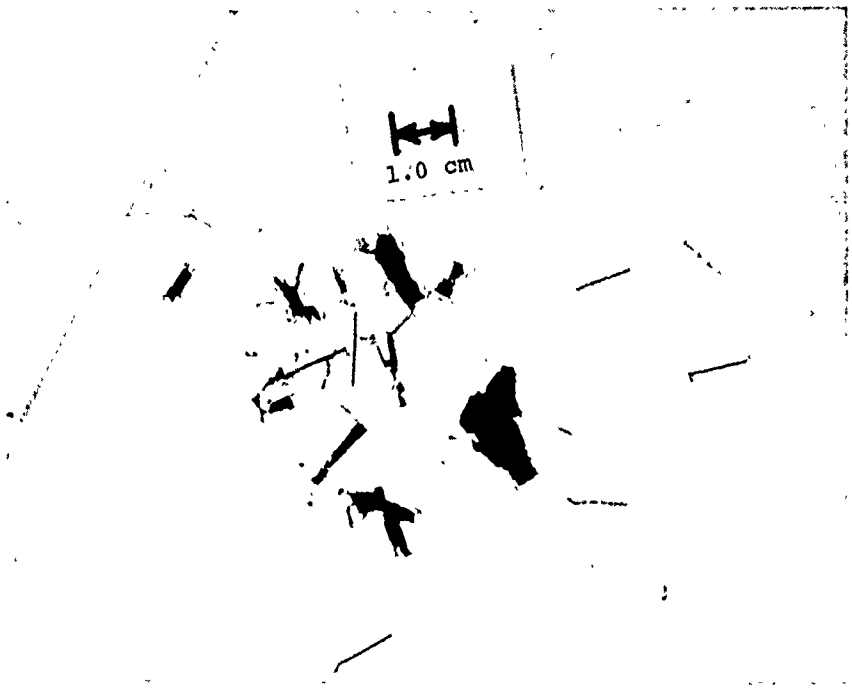

Figure 33. Post-Impact Pattern
Projectile: Axial Reinforced 40 Percent-0.04×10^{-2}m;
Velocity: 382 m/sec; Target: 0.016×10^{-2}m Aluminum

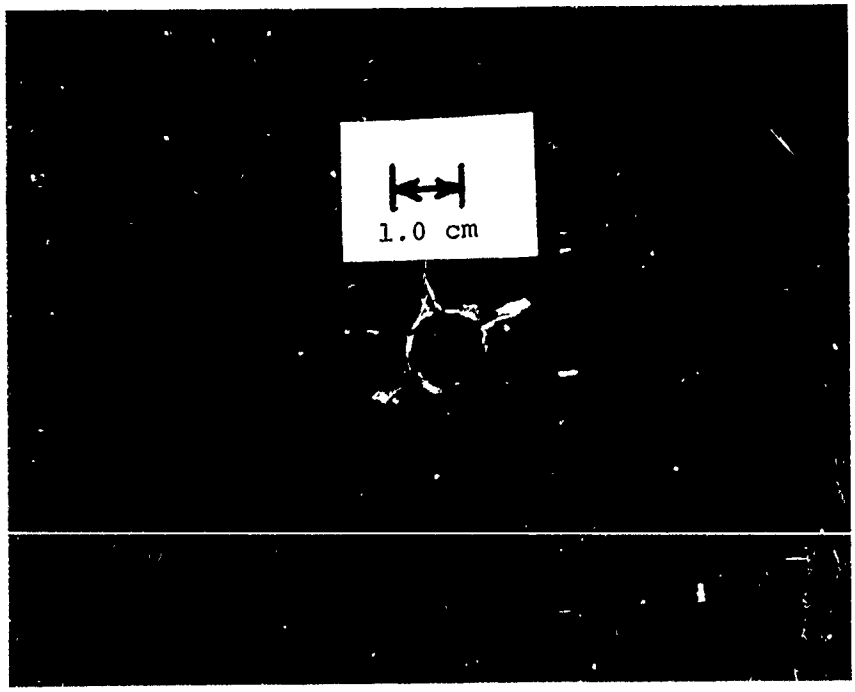

Figure 34. Plate Deformation Pattern
Projectile: Axial Reinforced 40 Percent-0.04×10^{-2}m;
Velocity: 381 m/sec; Target: 0.016×10^{-2}m Aluminum

Figure 35. Post-Impact Pattern
Projectile: Transverse Reinforced 10 Percent-0.04x10^{-2}m;
Velocity: 382 m/sec; Target: 0.016x10^{-2}m Aluminum

Figure 36. Post-Impact Pattern
Projectile: Transverse Reinforced 10 Percent-0.04x10^{-2}m;
Velocity: 382 m/sec; Target: 0.08x10^{-2}m Steel

Figure 37. Post-Impact Pattern
Projectile: Transverse Reinforced 25 Percent-0.04×10^{-2}m;
Velocity: 382 m/sec; Target: 0.16×10^{-2}m Aluminum

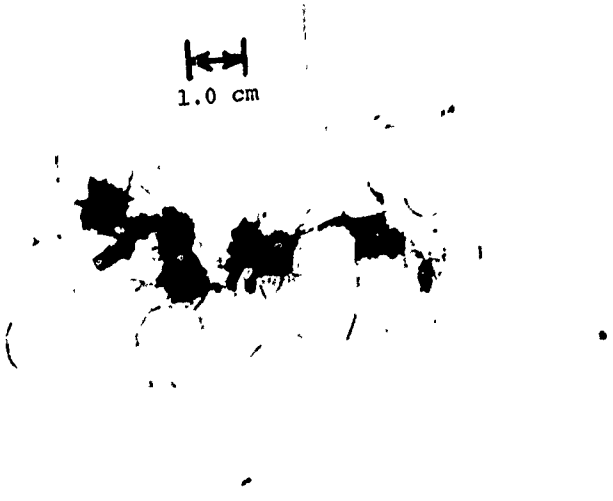

Figure 38. Post-Impact Pattern
Projectile: Transverse Reinforced 25 Percent-0.04×10^{-2}m;
Velocity: 382 m/sec; Target: 0.08×10^{-2}m Steel

Figure 39. Post-Impact Pattern
Projectile: Transverse Reinforced 40 Percent-0.04×10^{-2}m:
Velocity: 382 m/sec; Target: 0.16×10^{-2}m Aluminum

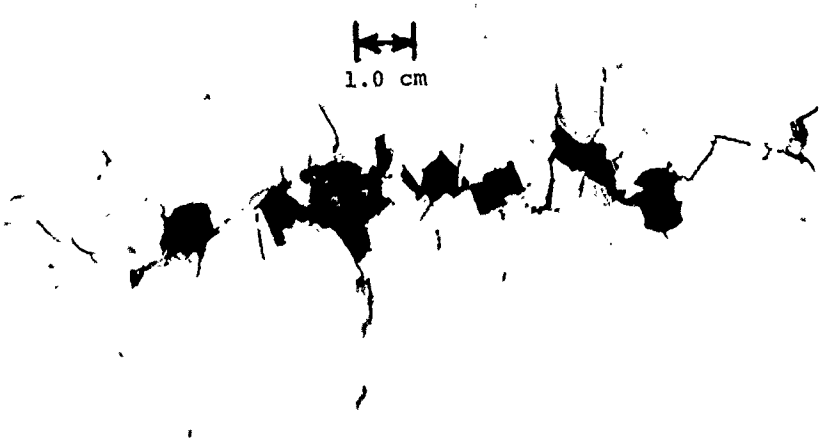

Figure 40. Plate Impact Pattern
Projectile: Transverse Reinforced 40 Percent-0.04×10^{-2}m;
Velocity: 382 m/sec; Target: 0.08×10^{-2}m Steel

The post-impact pattern of the 40 percent transverse reinforced specimens show an accentuated elongated pattern, as reproduced in Figure 39, for a 0.0016-meter aluminum plate and in Figure 40 for a 0.0008-meter steel plate. After considerable study of the preceding post-impact patterns and failure of the penetrated plate, it was observed that the filament alignment of the projectile filaments and the highly elongated fracture pattern were directly related.

Upon impact on the target the projectile has a tendency to deform in a uniform radial direction; however, due to the transverse orientation of the filaments the projectile is restrained from deformation in a direction parallel to the filament axes. (See x-x′ axis in Figure 41.) Deformation in the projectile along an axis (z-z′ of Figure 41) normal to the filament direction occurs and splitting, both longitudinally and transversely, as observed for impacts on massive targets, takes place in the specimen. The simultaneous fracturing of the projectile and bulging of the back side of the target plate continues until a shear plug failure occurs at the leading edge of the projectile. This plug is pushed ahead of the projectile, and the fracture specimen continues to expand in this normal direction causing petalling on two diametrically opposed sides of the penetration hole. This type of plate failure is shown for an aluminum plate in Figure 42 and for a steel plate in Figure 43. This plate failure pattern is in sharp contrast to the multiple petal failure observed for the axial reinforced projectile shown in Figure 34.

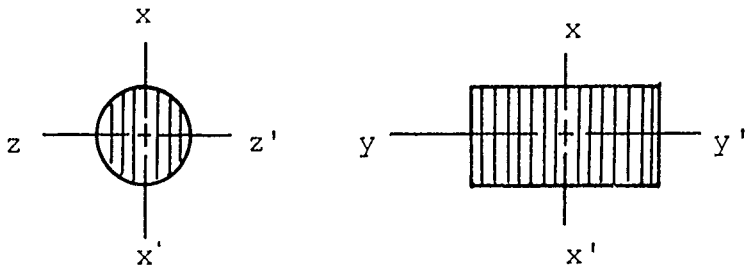

Figure 41. Filament Orientation of Transversely Reinforced Specimens

After penetration the fractured projectile continues to expand in a single direction causing a planar fan pattern shown in high-speed photographs (Figures 44 and 45) taken normal to this planar fan. These photographs were made possible by aligning the specimen in the gas gun barrel in such a manner as to control the post-impact pattern in plane normal to the

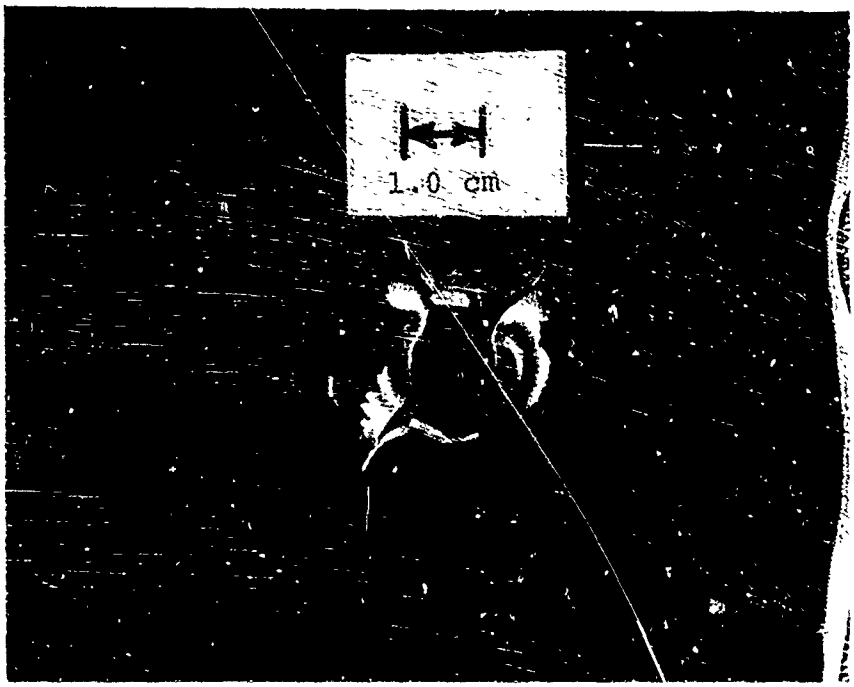

Figure 42. Plate Deformation Pattern
Projectile: Transverse Reinforced 40 Percent-0.04×10^{-2}m;
Velocity: 382 m/sec; Target: 0.16×10^{-2}m Aluminum

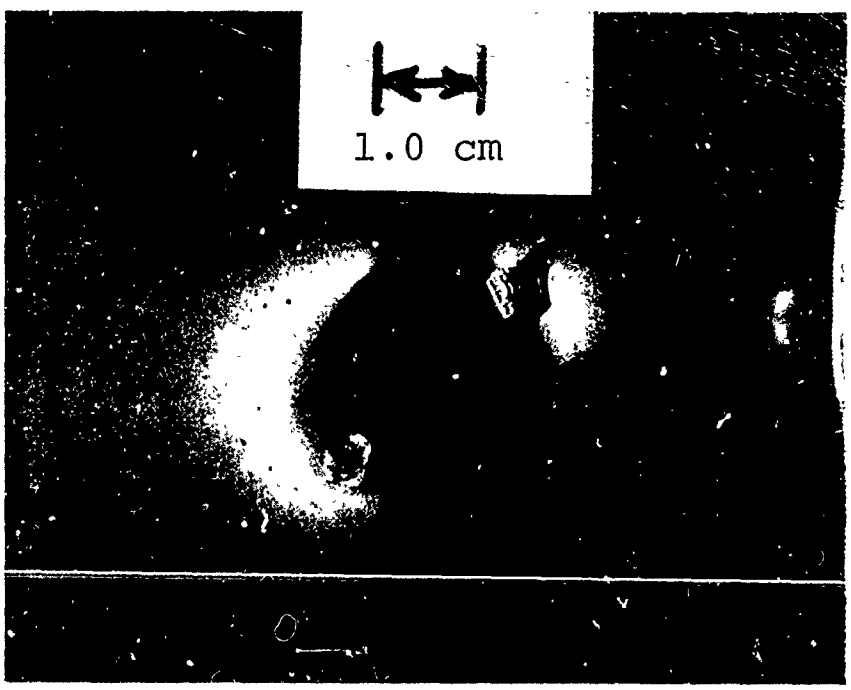

Figure 43. Plate Deformation Pattern
Projectile: Transverse Reinforced 40 Percent-0.04×10^{-2}m;
Velocity: 382 m/sec; Target: 0.16×10^{-2}m Aluminum

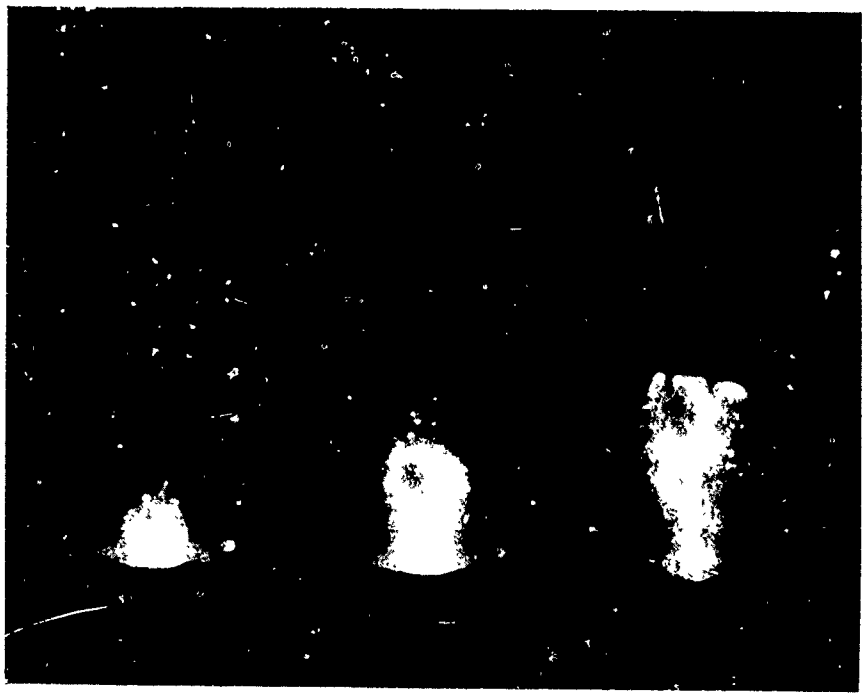

Figure 44. Post-Impact Projectile Fragmentation, 25 Percent Volume Fraction, 0.04×10^{-2}m Wire Diameter

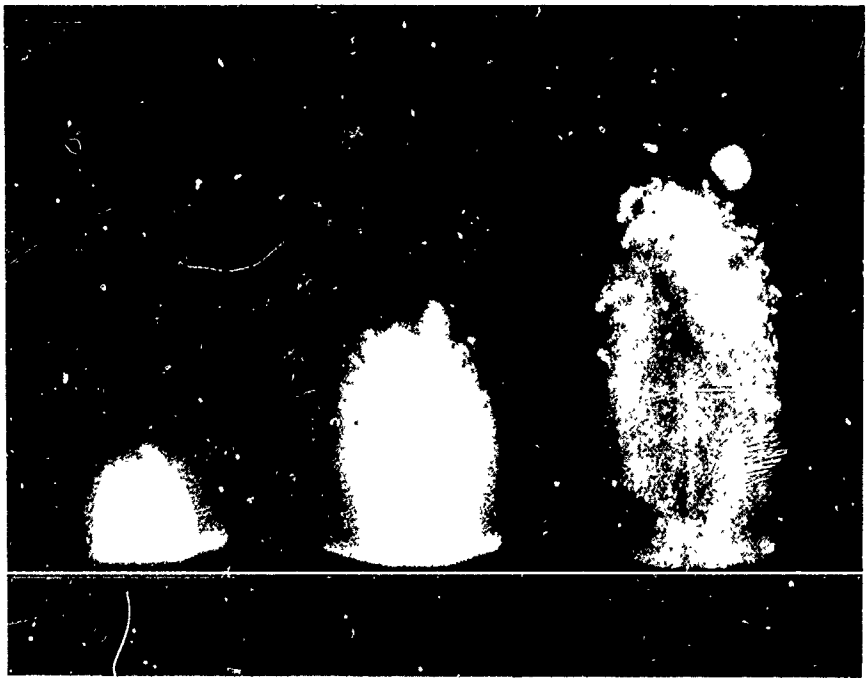

Figure 45. Post-Impact Projectile Fragmentation, 40 Percent Volume Fraction, 0.04×10^{-2}m Wire Diameter

camera. This planar fan pattern is continually expanding and causes the elongated post-impact pattern on the witness papers, as shown previously in Figures 37 to 40.

The difference in pattern size observed in both the high-speed photographs and on the witness paper may be attributed to (1) the kinetic energy of the 25 percent transverse reinforced specimen being much smaller than that of the 40 percent transverse specimens which results in a lower residual velocity observed in the high-speed photograph of Figure 44; and (2) the 40 percent transverse reinforced specimens are inherently more brittle and subject to greater cracking than the lower volume fraction specimens.

Tests performed on the very brittle concrete targets show that there is very little difference in fracture patterns for all types of filament-reinforced projectiles. Due to the brittle nature of the concrete target the interaction of the target-projectile combination is very different from that of the metal target-composite projectile combination. The large spall area of the target plate prevents the use of a witness paper for projectile fracture but from residual pieces taken from the styrofoam back indicates a rather random post-impact pattern for all composite projectiles tested.

3.4 Conclusions

From studies associated with plate impact and penetration mechanics the following conclusions are made:

(1) The critical velocity of composite-type materials for a given areal density was generally higher than mild steel plate material.

(2) Geometrical arrangement of fibers is extremely important in the resultant type of fracture pattern obtained. That is, either very localized or large interlaminar failures can occur based on ply geometry.

(3) For a single composite plate configuration, the geometrical ply arrangement is found to be important in optimizing energy-absorbing characteristics. This may be analogous and closely related to ply arrangement in statical deflection analysis.

(4) Brittle, low mass penetrators projected against ductile, high strength, high and low mass targets, break up more readily and result in larger post-impact fracture areas. These same penetrators projected at brittle, high mass. low strength targets tend to retain a greater degree of structural integrity.

(5) Controlled post-impact fracture patterns are obtained for transverse filament specimens projected against ductile, high strength, high and low mass targets. These fracture patterns are obtained for particular combinations of wire size, volume fractions, and firing velocities.

(6) Controlled fracture of a composite having a low shear strength matrix has been demonstrated. It appears that these results may be extended to other composite systems which have similar matrix properties.

APPENDIX I

DISCUSSION OF ANALYTICAL MODELS

To examine the influence of single lamina on propagating strain pulses, the analytical models discussed below have been examined. For both models considered, a knowledge of the interaction of a plane wave with a discontinuous boundary between two different media is required.

In order to introduce the first analytical model, consider the problem of a long bar of two dissimilar materials separated by an interface. Each media is assumed to be of uniform mechanical properties and is shown schematically in Figure I-1. In addition, it is assumed that the materials are perfectly elastic, a perfect interfacial bond exists, and a plane dilatational wave propagates through the media. The applicable wave equation is given by

$$\frac{\partial^2 y}{\partial x^2} = c^2 \frac{\partial^2 y}{\partial t^2} \tag{I-1}$$

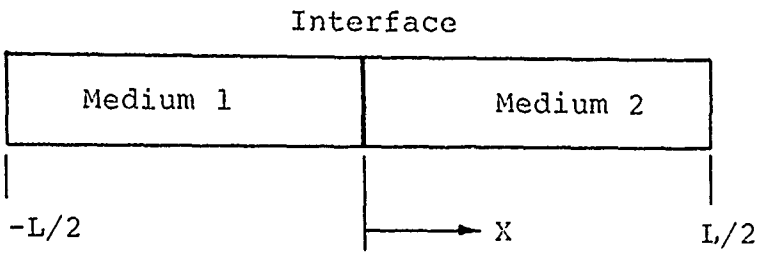

Figure I-1. Schematic of Uniform Bar with Dissimilar Materials

The boundary conditions to be satisfied at the interface are continuity of particle displacements and velocities expressed by

$$u_1 = u_2 \tag{I-2}$$

and

$$\frac{\partial u_1}{\partial t} = \frac{\partial u_2}{\partial t} . \tag{I-3}$$

At the interface, between the dissimilar media, part of the wave is transmitted and part reflected. Denote u_i as the displacement of the incident pulse, u_r as the displacement of the reflected pulse, and u_t as the displacement of the transmitted portion of the incident pulse. Substituting these into the boundary condition equations yields

$$u_i + u_r = u_t \tag{I-4}$$

and

$$\frac{\partial u_i}{\partial t} + \frac{\partial u_r}{\partial t} = \frac{\partial u_t}{\partial t} \, . \tag{I-5}$$

A general solution of the wave Equation (I-1) is given by,

$$u(x,t) = \varphi(t - \frac{x}{c}) + \psi(t + \frac{x}{c}) \tag{I-6}$$

where φ and ψ are arbitrary functions to be determined from the boundary conditions. The particle displacement of the incident pulse, assumed to be propagating from left to right in Figure I-1, is given by

$$u_i(x,t) = F(t - \frac{x}{c_1}) \tag{I-7}$$

where F is some known incident waveform. The reflected and transmitted particle displacements are then

$$u_r(x,t) = f_r(t + \frac{x}{c_1}) \tag{I-8}$$

and

$$u_t(x,t) = f_t(t - \frac{x}{c_2}) \tag{I-9}$$

where the subscript r refers to the reflected waveform and t refers to the transmitted waveform. Substituting the above displacement equations into the boundary equations gives the relations

$$F(t) + f_r(t) = f_t(t) \tag{I-10}$$

and

$$-\frac{F'(t)}{c_1} + \frac{f_r'(t)}{c_1} = -\frac{f_t'(t)}{c_2} \, . \tag{I-11}$$

Equation (I-11) can be integrated from time $t = 0$ to t, and solving simultaneously with Equation (I-10), to obtain expressions for f_r and f_t.

The two resulting relations, given below, are found to be functions of the acoustic velocities and incident wave form

$$f_r = \left[\frac{c_2 - c_1}{c_2 + c_1}\right] F \qquad \text{(I-12)}$$

$$f_t = \left[\frac{2c_2}{c_2 + c_1}\right] F \qquad \text{(I-13)}$$

To relate the above analysis to the physical problems of a distinct material lamina within a continuous bar material, the lamina is assumed to be a thin homogeneous-isotropic region (b); as shown in Figure I-2. Using this assumption, the modulus, density, and corresponding pulse propagation velocity are calculated from a rule of mixtures.

As the pulse impinges on the first interface e-e′, a transmission-reflection as described previously by Equations (I-12) and (I-13), respectively, exists. The transmitted portion of the pulse propagates th rough a region b of Figure I-2 until it impinges on the interface g-g′ where it once again undergoes a transmission-reflection process. The total pulse transmitted through the region b can be obtained by combining the results of the double transmission at interface e-e′ and g-g′, resulting in the following expression

$$F_t = \left[\frac{4c_e c_c}{(c_c + c_e)^2}\right] F \qquad \text{(I-14)}$$

where c_1 and c_2 have been replaced by the appropriate values of c_e for the acoustic velocity in epoxy and c_c for the acoustic velocity in the composite lamina.

Planar Composite Region

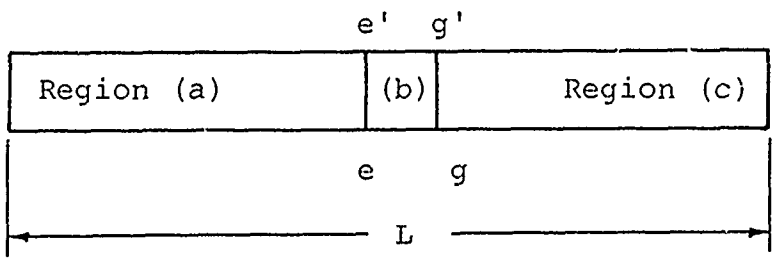

Figure I-2. Analytical Model of Single Composite Lamina

Equation (I-14) does not account for the reflected portion of the pulse at either of the interfaces, however, the portion of the pulse which is reflected from the g-g′ interface propagates in a negative direction through region b and impinges again on interface e-e′. Here it is again partially transmitted into region (a) and partially reflected back to interface g-g′ where the process is repeated. To obtain an expression for the pulse magnitude propagated into region (c), Equations (I-12) and (I-13) are applied successively, giving the result,

$$F_{2t} = \left[\frac{4c_e c_c (c_e - c_c)^2}{(c_e + c_c)^4}\right] F. \qquad \text{(I-15)}$$

It is assumed that the lamina thickness is small compared to the pulse length so that the second transmitted pulse described by Equation (I-15) superimposes with the pulse described by Equation (I-14) to form a new transmitted pulse. The internal reflection process continues until all of the energy has been transmitted out of the lamina; thus, the total transmitted pulse may be described by a series of superimposed transmission terms. After n internal transmission-reflection cycles, the total transmitted pulse magnitude is given as

$$F_{tn} = \frac{4c_e c_c}{(c_e + c_c)^2}\left[1 + \left(\frac{c_e - c_c}{c_e + c_c}\right)^2 + \ldots + \left(\frac{c_e - c_c}{c_e + c_c}\right)^{2n}\right] F. \qquad \text{(I-16)}$$

A transmission ratio can then be calculated by dividing through by F to nondimensionalize the equation.

This equation is used to calculate the lamina attenuations for the various different forms of the transmission-reflection model. The lamina attenuation (δ) is determined from the transmission ratio by the equation

$$\delta = \ell n \frac{F}{F_t} . \qquad \text{(I-17)}$$

As an alternate model formulation to the attenuation problem, a scattering model has been considered. This model is based upon the scattering of sound waves in air around a solid cylindrical body, which was first presented by Lord Rayleigh in Reference 21 and expanded upon by Morse in Reference 22. The latter has derived an approximate expression for the scattering of long wavelength acoustic waves around a non-sound conducting cylinder in air. This expression is given as

$$\pi_s = \left[\frac{6\pi^5 a^4}{\lambda^3}\right]\gamma_o \qquad \lambda \gg 2\pi a \qquad \text{(I-18)}$$

where

π_s is the total power scattered by the cylinder per unit length

a is the cylindrical radius

λ is the wavelength of the acoustic wave

γ_o is the initial intensity of the acoustic wave.

The total scattered power is given by π_s times the total length of cylinder upon which the wave front impinges. For the present analysis, the total cylinder length is given by the number of filaments in a lamina times the depth of the specimen cross section, denoted by the symbol L_f. The total power scattered by a lamina is then

$$P_{sT} = \pi_s L_f = \left[\frac{6\pi^5 a^4}{\lambda^3}\right]\gamma_o L_f \tag{I-19}$$

where P_{sT} is the total scattered power.

Initially, the total power of the pulse is given by its initial intensity (γ_o) times the specimen cross-sectional area A, that is,

$$P_{oT} = \gamma_o A \tag{I-20}$$

where P_{oT} is the total initial wave power.

It is assumed here that the propagating pulse loses all of its scattered power during transmission through the lamina; thus, the total transmitted power may be written as

$$P_{tT} = P_{oT} - P_{sT} = \left[A - \frac{6\pi^5 a^4 L_f}{\lambda^3}\right]\gamma_o \tag{I-21}$$

where P_{tT} is the total power of the pulse after transmission through the lamina.

On the basis of the preceding results, it is possible to define a power transmission ratio P_{tT}/P_{oT} or, dividing Equation (I-21) by Equation (I-20) to obtain

$$\frac{P_{tT}}{P_{oT}} = \left[1 - \frac{6\pi^5 a^4 L_f}{\lambda^3 A}\right]. \tag{I-22}$$

In Reference 22 it is noted that the wave power π is proportional to the square of the stress intensity which is, in turn, proportional to the

strain intensity under the governing assumption that stresses are in the linear elastic range. Symbolically, the result of these two proportionalities is written as

$$F = kP^{\frac{1}{2}} \tag{I-23}$$

where

F is strain amplitude
P is total power
k is a combination of constants.

Using Equation (I-23) an expression can be written for the strain amplitude transmission ratio used previously (Equation I-16) as

$$\frac{F_t}{F} = \left[1 - \frac{6\pi^5 a^4 L_f}{\lambda^3 A}\right]^{\frac{1}{2}} \quad (\lambda \gg 2\pi a) \tag{I-24}$$

where again L_f is the filament density times specimen cross-sectional depth.

Equation (I-24) characterizes the strain amplitude transmission ratio used in this report to calculate lamina attenuations based on the scattering model. Equation (I-17) was used to convert strain amplitude transmission ratios to lamina attenuation values as in the reflection-transmission model.

REFERENCES

1. Sierakowski, R. L., Nevill, G. E., Jr., Ross, C. A., and Jones, E. R., "Studies on the Ballistic Impact of Composite Materials," AFATL-TR-69-99, Air Force Armament Laboratory, Eglin Air Force Base, Florida, July 1969, UNCLASSIFIED.

2. Sierakowski, R. L., Nevill, G. E., Jr., Ross, C. A., and Jones, E. R., "Follow-on Studies of the Ballistic Impact of Composite Materials," AFATL-TR-70-87, Air Force Armament Laboratory, Eglin Air Force Base, Florida, August 1970, UNCLASSIFIED.

3. Burke, J. J. and Weiss, V., "Shock Waves and the Mechanical Properties of Solids," Syracuse University Press, Syracuse, New York, 1971, UNCLASSIFIED.

4. Friedrichs, K. O., The Theory of Wave Propagation, New York University Press, New York, 1953, UNCLASSIFIED.

5. Kolsky, H., Stress Waves in Solids, Dover Publications Inc., New York, 1963, UNCLASSIFIED.

6. Ashton, J. E., Halpin, J. C., and Petit, P. H., Primer on Composite Materials: Analysis, Technomic Publishing Co., Inc., Stamford, Connecticut, 1969, UNCLASSIFIED.

7. Broutman, L. J. and Krock, R. H., Modern Composite Materials, Addison-Wesley, Reading, Massachusetts, UNCLASSIFIED.

8. Kinslow, R., "Stress Waves in Laminated Materials," AIAA Paper No. 67-140, 1967, UNCLASSIFIED.

9. Pottinger, M. G., The Anisotropic Equivalent of the Love Longitudinal Wave Propagation Approximation, Aerospace Research Laboratory No. 70-0064, April 1970, UNCLASSIFIED.

10. Tauchert, T. R. and Guzelsu, A. N., "An Experimental Study of Dispersion of Stress Waves in a Fiber-Reinforced Composite," Journal of Applied Mechanics, ASME preprint paper no. 71-APM-27, UNCLASSIFIED.

11. Abbot, B. W. and Broutman, L. J., "Stress Wave Propagation in Composite Materials," Experimental Mechanics, July 1966, UNCLASSIFIED.

12. Tauchert, T. R. and Moon, F. C., "Propagation of Stress Waves in Fiber Reinforced Composite Rods," Proceedings of the 11th AIAA/AIME Structures, Structural Dynamics, and Materials Conference, Denver, Colorado, April 1970, UNCLASSIFIED.

13. Sierakowski, R. L., Nevill, G. E., Jr., Ross, C. A., and Jones, E. R., "Experimental Studies of the Dynamic Deformation and Fracture of Filament Reinforced Composites," Proceedings of the 11th AIAA/AIME Structures, Structural Dynamics, and Materials Conference, Denver, Colorado, April 1970, UNCLASSIFIED.

14. Ross, C. A., Cunningham, J. E., and Sierakowski, R. L., "Dynamic Wave Propagation in Transverse Layered Composites," Presented and published in Proceedings of the 42nd Shock and Vibration Symposium, Key West, Florida, November 1971.

15. Harris, C. M. and Crede, C. E. (Editors) Shock and Vibration Handbook, Volume 1, Section 7, McGraw-Hill Book Co., New York, 1961, UNCLASSIFIED.

16. Sierakowski, R. L., Nevill, G. E., Jr., Ross, C. A., and Jones, E. R., "Dynamic Compressive Strength and Failure of Steel Reinforced Epoxy Composites," Journal of Composite Materials, Volume 5, 1971, page 362.

17. Gupta, B. P. and Davids, N., "Penetration Experiments with Fiberglass-Reinforced Plastics," Experimental Mechanics, Volume 6, 1966, page 445, UNCLASSIFIED.

18. Wilkins, M. L., "Penetration Mechanics," Yale Scientific, Volume 44, 1970, page 16, UNCLASSIFIED.

19. Ruh, R., Stiglich, J. J., and Rankin, D. T., "Current and Potential Opaque Ceramic Armor Materials," Society of Aerospace and Materials Process Engineers Quarterly, Volume 2, 1971, page 46, UNCLASSIFIED.

20. Sedgwick, R. T., "Theoretical Terminal Ballistic Investigation and Studies of Impact at Low and Very High Velocities," AFATL-TR-68-61, Air Force Armament Laboratory, Eglin Air Force Base, Florida, May 1968, UNCLASSIFIED.

21. Rayleigh, B., The Theory of Sound, Dover Publications, New York, 1945, UNCLASSIFIED.

22. Morse, P. M., Vibration and Sound, McGraw-Hill Book Co., Inc., 1948, UNCLASSIFIED.

DOCUMENT CONTROL DATA - R & D

(Security classification of title, body of abstract and indexing annotation must be entered when the overall report is classified)

1 ORIGINATING ACTIVITY (Corporate author)
University of Florida
Gainesville, Florida

2a. REPORT SECURITY CLASSIFICATION
UNCLASSIFIED

2b. GROUP
--

3 REPORT TITLE

STUDIES OF THE DYNAMIC FRACTURE CHARACTERISTICS OF COMPOSITES

4 DESCRIPTIVE NOTES (Type of report and inclusive dates)
Final Report - January 1970 to January 1971

5 AUTHOR(S) (First name, middle initial, last name)
R. L. Sierakowski E. R. Jones
G. E. Nevill, Jr.
C. A. Ross

6 REPORT DATE	7a. TOTAL NO OF PAGES	7b. NO OF REFS
March 1972	75	22

8a. CONTRACT OR GRANT NO.
F08635-71-C-0076

b. PROJECT NO 2549

c. Task No. 03

d. Work Unit No. 002

9a. ORIGINATOR'S REPORT NUMBER(S)

9b. OTHER REPORT NO(S) (Any other numbers that may be assigned this report)
AFATL-TR-72-44

10 DISTRIBUTION STATEMENT
Distribution limited to U. S. Government agencies only; this report documents test and evaluation; distribution limitation applied March 1972. Other requests for this document must be referred to the Air Force Armament Laboratory (DLRD), Eglin Air Force Base, Florida 32542.

11 SUPPLEMENTARY NOTES
Available in DDC

12. SPONSORING MILITARY ACTIVITY
Air Force Armament Laboratory
Air Force Systems Command
Eglin Air Force Base, Florida 32542

13 ABSTRACT

The wave propagation behavior of composite bar specimens of variable fiber spacing and orientation is investigated. In addition, controlled geometry composite plates have been fabricated and impact tested to determine their failure/fracture characteristics. Wave propagation studies have been conducted on long rods with single filament lamina as well as continuous filament composite rods with variable filament orientation. A square wave input has been introduced into the rods, and wave speed, attenuation, and dispersion have been investigated. Analytical criteria have been considered to model a single lamina composite bar in order to isolate the influence of a single interface on wave speed, attenuation and dispersion. These results have been examined for correlation with multiple filament rods. Various geometry plate specimens have been fabricated and impact tested to determine their energy-absorbing characteristics and failure/fracture modes. Further, penetrator specimens of a model composite geometry type have been impact tested against variable density targets to investigate the possibility of producing controlled fracture characteristics.

DD FORM 1 NOV 65 1473

14 KEY WORDS	LINK A		LINK B		LINK C	
	ROLE	WT	ROLE	WT	ROLE	WT
Dynamic Compressive Behavior						
Unidirectional Reinforced Composite Specimens						
Transversely Reinforced Composite Specimens						
Non-Metal Reinforced Systems						
Failure/Fracture Studies						
Ballistic Impact						
Plate Penetration						
Wave Propagation Behavior						
Wave Attenuation						
Wave Dispersion						